ELSEVIER

Journal of Fluids and Structures 21 (2005) 485–529

JOURNAL OF FLUIDS AND STRUCTURES

www.elsevier.com/locate/jfs

Triggering mechanisms of limit cycle oscillations due to aeroelastic instability

Y.S. Lee[a], A.F. Vakakis[a,b,c], L.A. Bergman[c,*], D.M. McFarland[c], G. Kerschen[d]

[a]*Department of Mechanical and Industrial Engineering, University of Illinois at Urbana-Champaign, USA*
[b]*Department of Applied Mathematical and Physical Sciences, National Technical University of Athens, USA*
[c]*Department of Aerospace Engineering, University of Illinois at Urbana-Champaign, 104 South Wright Street, 321E Talbot Laboratory, Urbana, IL 61801, USA*
[d]*Département d'Aérospatiale, Mécanique et Matériaux (ASMA), Université de Liège, USA*

Received 5 May 2005; accepted 4 August 2005

Abstract

We show that a cascade of resonance captures constitutes the triggering mechanism of limit cycle oscillations (LCOs) due to aeroelastic instability of rigid wings in flow. We consider a two-degree-of-freedom (2-dof) wing model in subsonic flow with cubic nonlinear stiffnesses at the support. Under the assumption of quasi-steady aerodynamics, we apply a complexification/averaging technique to express the dynamics of fluid–structure interactions in terms of three fast-frequency components; these are the two linear natural frequencies corresponding to heave and pitch, and a super-harmonic at three times the pitch frequency. Bifurcation analysis of the resulting set of modulation equations governing the slow dynamics is carried out via the method of numerical continuation, and reveals the different types of steady state motions realized as parameters vary. It turns out that the LCO triggering mechanism consists of a combination of different dynamic phenomena, taking place at three main stages or regimes: attraction to transient resonance captures (TRCs), escapes from these captures and, finally, entrapments into permanent resonance captures (PRCs). We examine numerically and analytically the dynamics at each of these stages by means of wavelet transform analysis, study of the evolution of appropriately defined phase variables in projections of the phase space of the dynamics, and analysis of instantaneous energy exchanges between the various nonlinear modes involved. The general conclusion is that an initial excitation of the heave mode by the flow acts as the triggering mechanism for the excitation of the pitch mode through nonlinear interactions resulting from the resonance captures and escapes. The eventual excitation of the pitch mode signifies the appearance of an LCO of the in-flow wing.

Keywords: Limit cycle oscillation (LCO); Aeroelastic instability; Numerical continuation; Triggering mechanism; Resonance capture

1. Introduction

We study triggering mechanisms for limit cycle oscillations (LCOs) due to aeroelastic instability in a two-dimensional, two-degree-of-freedom (dof) wing model with cubic nonlinear structural stiffnesses in both dof (i.e., heave

*Corresponding author. Tel.: +1 217 3334970; fax: +1 217 2440720.
E-mail addresses: yslee4@uiuc.edu (Y.S. Lee), vakakis@central.ntua.gr, avakakis@uiuc.edu (A.F. Vakakis), lbergman@uiuc.edu (L.A. Bergman), dmmcf@uiuc.edu (D.M. McFarland), g.kerschen@ulg.ac.be (G. Kerschen).

0889-9746/$ - see front matter © 2005 Elsevier Ltd. All rights reserved.
doi:10.1016/j.jfluidstructs.2005.08.011

and pitch), under the assumptions of subsonic flight and quasi-steady aerodynamics. Fundamentals of the flutter analysis for the underlying linear model are well-known [see, for example, Fung (1955) and Dowell et al. (1995)]; i.e., instability due to Hopf bifurcation at the flutter speed leading to diverging responses. However, due to structural or damping nonlinearities, such divergence in the linear model can be limited so that, eventually, the system attains self-sustaining responses in the form of LCOs (Nayfeh and Mook, 1979).

LCOs are known to be a persistent problem on fighter aircraft such as the F-16 and F/A-18 at high subsonic and transonic speeds (Bunton and Denegri, 2000). The interaction between wing and store of a parametric F-16 wing was studied numerically by combining the finite element method and computational fluid mechanics (Cattarius, 1999). Flight tests were performed to measure actual LCOs of these fighters (Denegri, 2000). Lee and LeBlanc (1986) numerically examined the effects of cubic nonlinear stiffness on the flutter behavior of a two-dimensional airfoil. They established that when the system has softening stiffness, it may possess subcritical LCOs which occur below the linear flutter speed so that they show dependence on initial conditions; for a hardening spring, however, such dependence on initial conditions disappears, and a single LCO is obtained for a single value of the flow speed. Lee and Desrochers (1987) considered different kinds of structural nonlinearities, such as free play (i.e., dead-zone nonlinearity), for flutter analysis. The existence of LCOs of prototypical aeroelastic wing sections with torsional nonlinearity including asymmetry was studied using the describing function method, and it was shown that the amplitude of a pitching LCO does not always increase with the flow speed for certain elastic axis positions (Singh and Brenner, 2003). Computational and experimental studies of LCOs in nonlinear aeroelastic systems were also performed (O'Neil and Strganac, 1998; Sheta et al., 2002); in particular, Sheta et al. (2002) employed a multidisciplinary analysis to compare numerical with experimental data, suggesting the importance of modeling both the fluid and structural nonlinearities for accurate prediction of the onset and the magnitudes of LCOs. Normal form theory was utilized to investigate and unfold the subcritical/supercritical nature of the flutter Hopf bifurcation (Coller and Chamara, 2004); and a higher-order harmonic balance method was considered to study the secondary Hopf bifurcation of aeroelastic responses (Liu and Dowell, 2004). Gilliatt et al. (2003) studied the possibility of internal resonance in an aeroelastic system (a stall model) under nonlinear aerodynamic loads; and Lind et al. (2001) utilized a wavelet transform to model structural nonlinearities from flight data, and used its results to predict the onset of LCOs.

Many studies have attempted to analyze flutter behavior and the resulting LCOs; however, no works have focused on the modeling and physical understanding of the LCO triggering mechanism itself. The classical notion of flutter from linear analysis is that '… *lift inputs energy into heave and pitch lags by* 90°; *flutter is a combination of the pitch and heave modes with phase and amplitude that extracts energy from the flow when either mode acting alone would be stable* …' (Fung, 1955). Thus, the main objective of this study is to understand the LCO triggering mechanism considering the simplest adequate model; i.e., the study of the dynamics of how the LCOs are triggered, and then developed, in a wing model containing cubic nonlinear structural stiffness in both dof (heave and pitch).

We start with the system description in Section 2, together with linear flutter analysis results which can be found in references such as Dowell et al. (1995); in Section 3, we first examine dominant frequency components via fast Fourier transforms (FFTs), and characterize their instantaneous variation via wavelet transforms (WTs) with respect to a reduced velocity; then we develop the slow-flow dynamics model based on numerical observations; and finally we establish a multiphase averaged system (Lochak and Meunier, 1988) with three main frequency components utilizing the complexification/averaging technique first developed by Manevitch (2001). Then, we present steady-state bifurcation analysis utilizing *MATCONT*, which is the numerical continuation code in Matlab® developed by Dhooge et al. (2003). In Section 4, after reviewing some useful definitions and theories, we numerically study the LCO triggering mechanisms from the slow-flow dynamics model. It turns out that the mechanism is composed of a series of *transient and permanent resonance captures* (Burns and Jones, 1993; Vakakis and Gendelman, 2001), through which energy transfers between modes occur. Eventually, energy balance is reached, leading to steady-state periodic motions, or LCOs. Then, the partially averaged systems (Arnold, 1988) derived at each stage constitute reliable analytical models that are used to study the resonance capture phenomena which accompany *frequency shifting* (Zniber and Quinn, 2003) in the response due to fluid–structure interaction with increase of input energy. Finally, concluding remarks are presented.

2. System description

Consider a two-dimensional rigid wing model with two dof: heave and pitch (Fig. 1). In Fig. 1, we denote by **ac** the aerodynamic center (usually assumed to be located at a quarter-chord); by **ea**, the elastic axis; by **cg**, the center of gravity; by h and α, heave (positive downward) and pitch (positive clockwise) dofs, respectively; by $c = 2b$, the chord

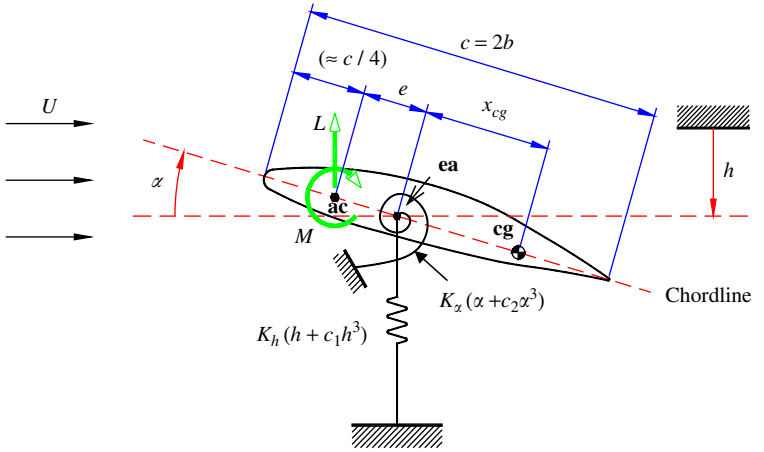

Fig. 1. Two-dimensional, two-degree-of-freedom wing model.

length; by e, the location of the **ac** measured from the **ea** (positive forward of **ea**); by x_{cg}, location of the **cg** measured from the **ea** (positive aft of the **ea**); by K_h and K_α, the linear bending and twist stiffness coefficients, respectively; by c_1 and c_2, the nonlinear bending and twist stiffness factors, respectively; by U, (constant and uniform) flow speed around the wing; by L and M, lift and aerodynamic moment respectively acting at the **ac** so that equivalent aerodynamic forces acting at the **ea** can be computed as $L_{ea} = L, M_{ea} = M + eL \approx eL$ for small angles.

Referring to Dowell et al. (1995), we write the equations of motion

$$\begin{aligned} &m\ddot{h} + S_\alpha\ddot{\alpha} + K_h(h + c_1h^3) + qS\frac{\partial C_L}{\partial\alpha}\left(\alpha + \frac{\dot{h}}{U}\right) = 0,\\ &I_\alpha\ddot{\alpha} + S_\alpha\ddot{h} + K_\alpha(\alpha + c_2\alpha^3) - qSe\frac{\partial C_L}{\partial\alpha}\left(\alpha + \frac{\dot{h}}{U}\right) = 0, \end{aligned} \tag{1}$$

where m is the mass of the airfoil; S_α, the mass unbalance; I_α, the mass moment of inertia with respect to **ea**; q, the dynamic pressure; and S, the almost invariable planform area of the wing. The differentiation indicated by the over-dot is with respect to time, t. Quasi-steady aerodynamics is assumed so that we have the lift $L = qS(\partial C_L/\partial\alpha)(\alpha + \dot{h}/U)$.

In nondimensional form the equations of motion are

$$\begin{aligned} &y'' + x_\alpha\alpha'' + \mu C_{L,\alpha}\Theta y' + \Omega^2 y + \xi_y y^3 + \mu C_{L,\alpha}\Theta^2\alpha = 0,\\ &r_\alpha^2\alpha'' + x_\alpha y'' - \mu\gamma C_{L,\alpha}\Theta y' + (r_\alpha^2 - \mu\gamma C_{L,\alpha}\Theta^2)\alpha + \xi_\alpha\alpha^3 = 0, \end{aligned} \tag{2}$$

where $y = h/b$ is the nondimensional heave motion; $x_\alpha = S_\alpha/(mb) = x_{cg}/b$, the nondimensional static unbalance; $\Omega = \omega_h/\omega_\alpha$, the ratio of uncoupled linear natural frequencies $\omega_h = \sqrt{K_h/m}$ and $\omega_\alpha = \sqrt{K_\alpha/I_\alpha}$; $\mu = \rho_\infty bS/(2m)$, the density ratio; $C_{L,\alpha} = \partial C_L/\partial\alpha$, the slope of the lift coefficient at zero angle of attack; $\Theta = U/(b\omega_\alpha)$, the reduced speed of the flow; r_α, the radius of gyration of the cross-section of the wing; $\gamma = e/b$, the nondimensional distance of the **ea** from the **ac**; and ξ_y and ξ_α, the respective coefficients for the nonlinear stiffness terms. Differentiation in (2) is with respect to the nondimensional time, $\tau = \omega_\alpha t$.

First, we perform a linearized analysis by substituting $y = e^{p\tau}\bar{y}$, $\alpha = e^{p\tau}\bar{\alpha}$ into (2), and considering only the linear part of (2) (i.e., we set $c_1 = c_2 \equiv 0$); hence, we obtain the following linearized complex eigenvalue problem:

$$\begin{bmatrix} p^2 + \mu C_{L,\alpha}\Theta p + \Omega^2 & x_\alpha p^2 + \mu C_{L,\alpha}\Theta^2 \\ x_\alpha p^2 - \mu\gamma C_{L,\alpha}\Theta p & r_\alpha^2 p^2 + r_\alpha^2 - \mu\gamma C_{L,\alpha}\Theta^2 \end{bmatrix} \begin{pmatrix} \bar{y} \\ \bar{\alpha} \end{pmatrix} = \begin{pmatrix} 0 \\ 0 \end{pmatrix}. \tag{3}$$

The linearized solvability condition for the complex frequency equation becomes,

$$A_4p^4 + A_3p^3 + A_2p^2 + A_1p + A_0 = 0, \tag{4}$$

where

$$A_4 = r_\alpha^2 - x_\alpha^2, A_3 = \mu C_{L,\alpha}\Theta(r_\alpha^2 + \gamma x_\alpha), \quad A_2 = r_\alpha^2(1+\Omega^2) - \mu C_{L,\alpha}(x_\alpha + \gamma)\Theta^2,$$
$$A_1 = \mu r_\alpha^2 C_{L,\alpha}\Theta, A_0 = \Omega^2(r_\alpha^2 - \mu\gamma C_{L,\alpha}\Theta^2).$$

Using the parameters from Dowell et al. (1995),

$$x_\alpha = 0.2, \quad r_\alpha = 0.5, \quad \gamma = 0.4, \quad \Omega = 0.5, \quad \mu = (10\pi)^{-1}, \quad C_{L,\alpha} = 2\pi, \quad \xi_y = \xi_\alpha \equiv 1, \tag{5}$$

we perform linearized flutter analysis to compute the flutter speed at which divergent responses are predicted.

Fig. 2 shows the real and imaginary parts of the solution $p = p_R + i\omega$ ($p_R, \omega \in \mathbb{R}$) of (4). The real part p_R determines the stability of the trivial equilibrium; if $p_R > 0$, the solution is unstable, which implies divergent response of the wing. For the above numerical parameter values, we obtain the flutter speed $\Theta_F^{(QS)} = \Theta_F = 0.87$. Note that steady aerodynamics predicts a higher flutter speed than quasi-steady theory (i.e., $\Theta_F^{(S)} = 1.03$), and also the frequency coalescence at the flutter speed for the steady flow condition. This is called *coalescence* or *merging frequency flutter* (Dowell et al., 1995).

Now we include nonlinear stiffnesses in both dof. Clearly, stability behavior of the trivial solution $y = \alpha \equiv 0$ will follow the linear analysis since the trivial solution is a hyperbolic equilibrium point, so we can invoke the Hartman-Grobman Theorem and claim topological conjugacy between the linear and nonlinear local vector fields sufficiently close to the hyperbolic equilibrium (Guckenheimer and Holmes, 1983). Also, due to the hardening nonlinearities, which are expected to limit the amplitudes of the responses, the nonlinear system may possess LCOs at supercritical speeds (i.e., for $\Theta > \Theta_F$). In Fig. 3 we depict typical responses at subcritical and supercritical speeds of the linearized and nonlinear system (2), respectively. We see that the linear system predicts divergent responses, which are clearly not realistic; in actuality, the nonlinearities restrict the growth of the diverging wing so that LCOs are developed instead.

3. Slow-flow dynamics

3.1. Frequency information with respect to reduced velocity

In order to establish an accurate slow-flow dynamics model that captures reliably and robustly the full nonlinear response of system (2), we need to determine precisely the dominant frequency components of the dynamics in the

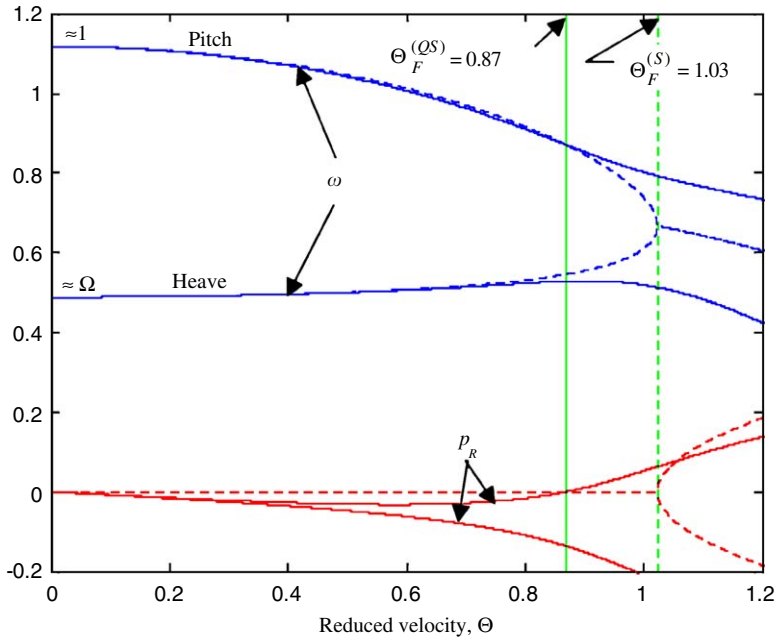

Fig. 2. Real and imaginary parts of the solutions of Eq. (4) with respect to the reduced velocity; solid and dashed lines correspond to the eigenvalues computed by using quasi-steady (QS) and steady (S) aerodynamics, respectively.

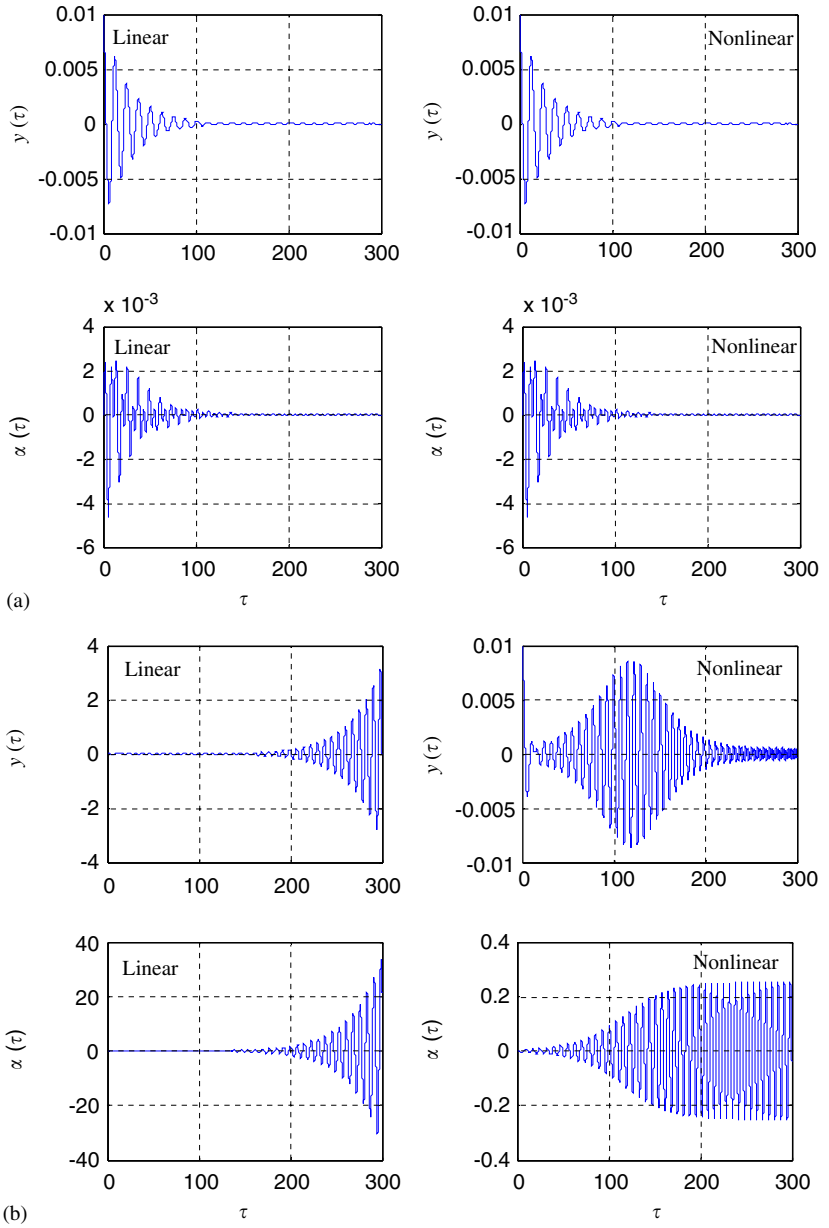

Fig. 3. Time responses at (a) subcritical ($\Theta = 0.5$) and (b) supercritical ($\Theta = 0.95$) reduced velocities in the linear and nonlinear models; initial conditions are $(y(0), \alpha(0), y'(0), \alpha'(0)) = (0.01, 0, 0, 0)$.

different stages of the motion; see, for example, Lee et al. (2005) regarding an analytical study of the symmetric and unsymmetric periodic solutions of an essentially nonlinear system, containing multifrequency components. Determination of the dominant frequency components in the nonlinear response is important, as it will dictate the dimensionality of the reduced order model that will be developed to model the nonlinear dynamics.

First, we examine the dominant frequency components in the responses for varying reduced velocity. Fig. 4 presents power spectra of the heave and pitch responses normalized with their respective maximum power at each reduced velocity. For subcritical reduced speeds (i.e., $\Theta < \Theta_F$), there are only two dominant frequency components, ω_{heave} and ω_{pitch}, related to the two linearized natural frequencies for the heave and pitch (in terms of the nondimensional frequencies defined previously the two dominant components are Ω and 1, respectively). When the reduced velocity

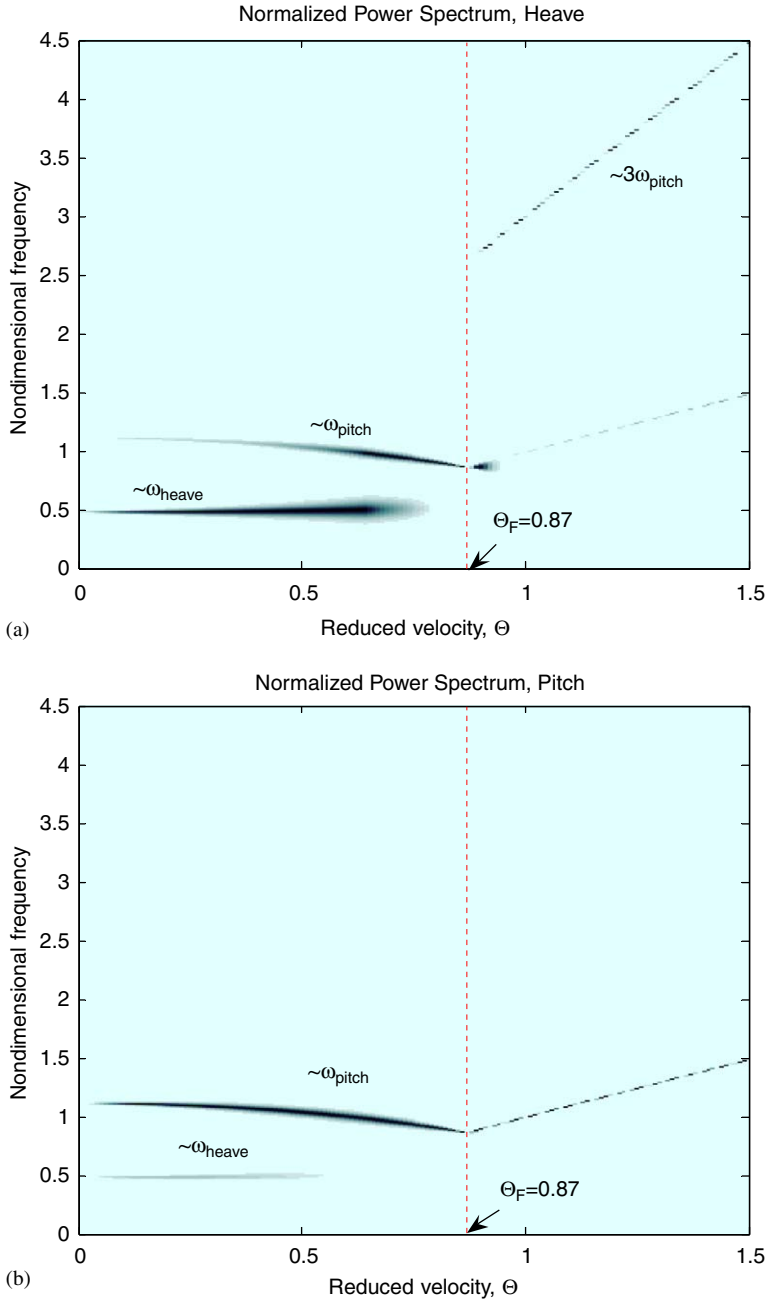

Fig. 4. Normalized power spectrum with respect to the reduced velocity: (a) heave and (b) pitch (ω_{heave} and ω_{pitch} denote frequency components close to the linear natural frequencies of heave and pitch, respectively; i.e., $\omega_{\text{heave}} \approx \Omega = 0.5$ and $\omega_{\text{pitch}} \approx 1$); initial conditions are $(y(0), \alpha(0), y'(0), \alpha'(0)) = (0.01, 0, 0, 0)$.

exceeds the flutter speed (i.e., $\Theta > \Theta_F$), there appear two dominant frequency components, ω_{pitch} and $3\omega_{\text{pitch}}$, for the heave mode; and one dominant frequency component, ω_{pitch}, for the pitch mode. This clearly shows that below and above the flutter speed, the aeroelastic response of the wing contains three dominant frequency components, related to the two linear natural frequencies of the linear flutter model; that is, the lowest component corresponds to the heave mode (i.e., $\omega_{\text{heave}} \approx \Omega = 0.5$), the middle one to the pitch mode (i.e., $\omega_{\text{pitch}} \approx 1$), and the highest one is approximately three times that of the pitch mode (i.e., $3\omega_{\text{pitch}} \approx 3$). In the following exposition we will refer to these three dominant frequencies by LF, MF, and HF (low, middle, and high frequencies), respectively.

The FFT analysis provides an averaged view of the frequency content of a signal. Since the phenomena studied in this work are essentially nonlinear and transient, we resort instead to frequency decompositions based on wavelet transforms (WTs), which provide information on the temporal evolutions of the dominant harmonic components of the subcritical or supercritical transient responses of the wing. This will enable us to clearly establish and study transitions that occur between different regimes of the transient motions. For clarity, we review the WT analysis which was also used in Lee et al. (2005). The WT can be viewed not only as a basis for functional representation, but at the same time as a useful technique for time-frequency analysis (Keener, 2000); the WT involves a windowing technique with variable-sized regions so that it may perform a multi-resolution analysis, in contrast to the FFT which assumes signal stationarity as aforementioned. Small time intervals are considered for high-frequency components whereas the size of the interval is increased for lower-frequency components, thereby giving better time and frequency resolutions than the FFT. The Matlab® codes used for the WT computations in this work were developed at the Université de Liège by Dr V. Lenaerts in collaboration with Dr P. Argoul from the Ecole Nationale des Ponts et Chaussées (Paris, France). Two types of mother wavelets $\psi_M(t)$ are considered in the codes: (i) the Morlet wavelet, which is a Gaussian-windowed complex sinusoid of frequency ω_0, $\psi_M(t) = e^{-t^2/2} e^{j\omega_0 t}$; and (ii) the Cauchy wavelet of order n, $\psi_M(t) = [j/(t+j)]^{n+1}$, where $j^2 = -1$. The frequency ω_0 for the Morlet WT and the order n for the Cauchy WT are user-specified parameters which allow one to tune the frequency and time resolutions of the results. In this study, we utilized the Morlet wavelet. The plots shown represent the amplitude of the WT as a function of frequency (vertical axis) and time (horizontal axis). Heavy shaded areas correspond to regions where the amplitude of the WT is high whereas lightly shaded regions correspond to low amplitudes. Such plots enable one to deduce the temporal evolutions of the dominant frequency components of the signals analyzed.

We perform WT analysis for two specific reduced velocities; $\Theta = 0.5$ and 0.95 corresponding to subcritical and supercritical wing responses, respectively (Figs. 5 and 6). However, the results presented herein can be extended to other values corresponding of subcritical or supercritical reduced speeds.

When the flow speed is less than the flutter speed (i.e., in a subcritical regime), the linear natural frequency of the heave mode appears as the main frequency component in heave, and that of the pitch mode as the minor. On the other hand, the pitching response possesses both heave and pitch harmonics with the pitch harmonic being the dominant one. Apparently, there exists a frequency relation of $\omega_{\text{pitch}} \approx 2\omega_{\text{heave}}$ as we may expect from the relation satisfied by the two linear natural frequencies; i.e., a 1:2 internal resonance occurs in the transient dynamics of the wing when a flow speed is less than the flutter speed. In addition, we can see existence of the non-negligible frequency component in the pitch mode at the linearized heave natural frequency (i.e., $\approx \Omega = 0.5$) so that the lowest likewise frequency components both in heave and pitch modes appear to interact with each other up to $\tau \approx 80$. In Section 4.2, we will show numerically that this transient dynamics is also captured into a 1:1 resonance manifold (Quinn, 1997a; Vakakis and Gendelman, 2001). Clearly, the energy extracted from the flow is being channeled and then exchanged between the nonlinear modes through resonance captures (as discussed below).

In the supercritical regime, however, a qualitative change in the dynamics occurs, since a sudden transition (jump) between frequency components takes place. To understand such transitions we will need to partition the dynamics into three separate phases: (i) an initial transient period, where likewise frequency components are likely to match each other leading to 1:1 resonance captures (we will define this dynamical mechanism leading to rigorous energy exchanges between interacting nonlinear modes, as transient resonance capture, or TRC); (ii) a transition or escape phase into new frequency or resonance relations, where the basic heave harmonic gradually triggers the pitch mode at its dominant harmonic and then dies out, whereas at the same time a higher frequency component develops nearly at three times the pitch linearized frequency (i.e., a 3:1 super-harmonic component); and finally (iii) generation of LCOs as a steady-state response develops, where the resulting dominant harmonics are the 3:1 super-harmonic component in heave mode and the pitch linearized frequency in pitch mode. We will explore each one of these phases of the dynamics in detail, since they constitute triggering mechanism for LCOs in the in-flow rigid wing.

3.2. Multiphase averaged system

Before proceeding to the analysis of the different regimes of the triggering mechanism, it will be necessary to develop a reduced order model of the dynamics through multiphase averaging, taking into account the previous WT-based frequency analysis. To this end, we reconsider the equations of motion (2), and through a linear coordinate transformation express them in the following inertially decoupled form,

$$\begin{aligned} &y'' + \zeta_1 y' + k_{11} y + k_{12}\alpha + n_{11} y^3 + n_{12}\alpha^3 = 0,\\ &\alpha'' + \zeta_2 y' + k_{21} y + k_{22}\alpha + n_{21} y^3 + n_{22}\alpha^3 = 0, \end{aligned} \tag{6}$$

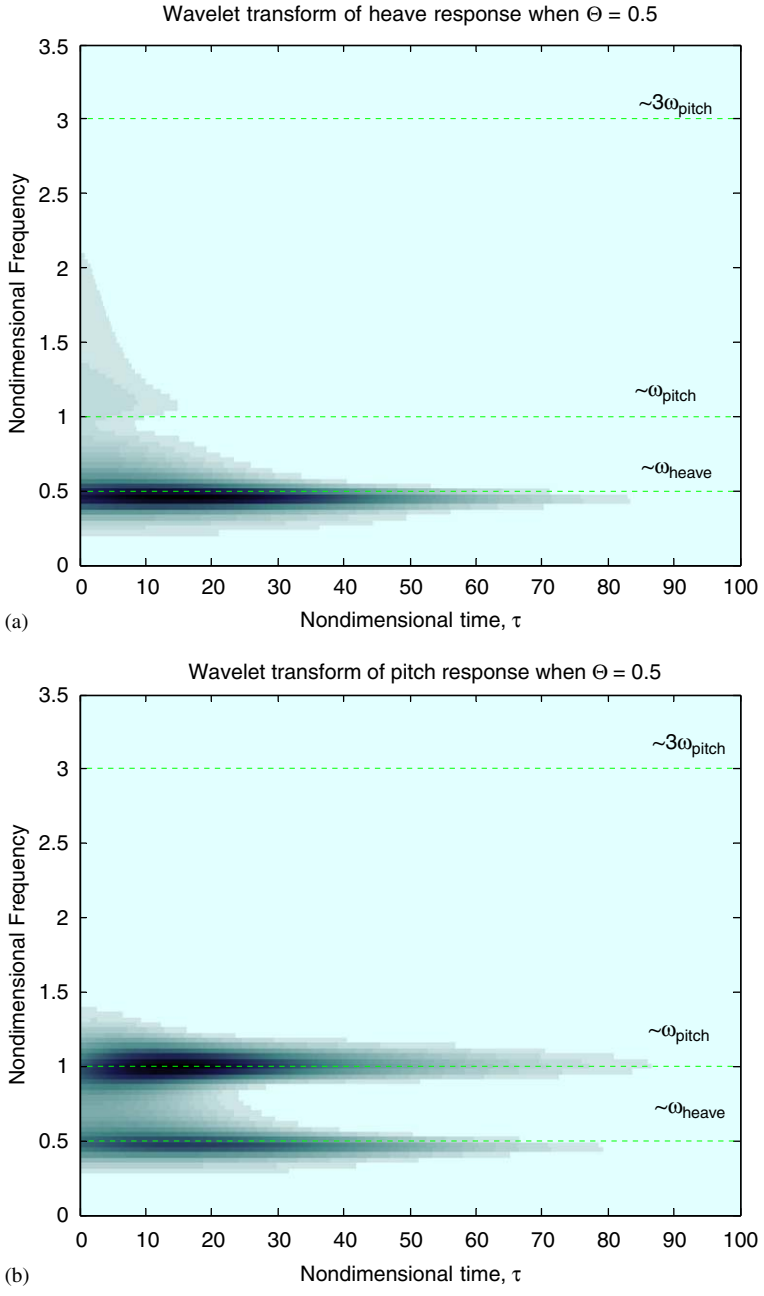

Fig. 5. Time-dependent frequency responses at a subcritical speed ($\Theta = 0.5$): (a) heave and (b) pitch; initial conditions are $(y(0), \alpha(0), y'(0), \alpha'(0)) = (0.01, 0, 0, 0)$.

where the coefficients are defined as

$$\begin{aligned}
&\zeta_1 \equiv \mu C_{L,\alpha}\Theta(r_\alpha^2 + \gamma x_\alpha)/D, \quad \zeta_2 \equiv -\mu C_{L,\alpha}\Theta(\gamma + x_\alpha)/D,\\
&k_{11} \equiv r_\alpha^2\Omega^2/D, \quad k_{12} \equiv \{\mu C_{L,\alpha}\Theta^2(r_\alpha^2 + \gamma x_\alpha) - r_\alpha^2 x_\alpha\}/D,\\
&k_{21} \equiv -x_\alpha\Omega^2/D, \quad k_{22} \equiv \{r_\alpha^2 - \mu C_{L,\alpha}\Theta^2(\gamma + x_\alpha)\}/D,\\
&n_{11} \equiv r_\alpha^2\xi_y/D, \quad n_{12} \equiv -x_\alpha\xi_\alpha/D, \quad n_{21} \equiv -x_\alpha\xi_y/D, \quad n_{22} \equiv \xi_\alpha/D
\end{aligned} \tag{7}$$

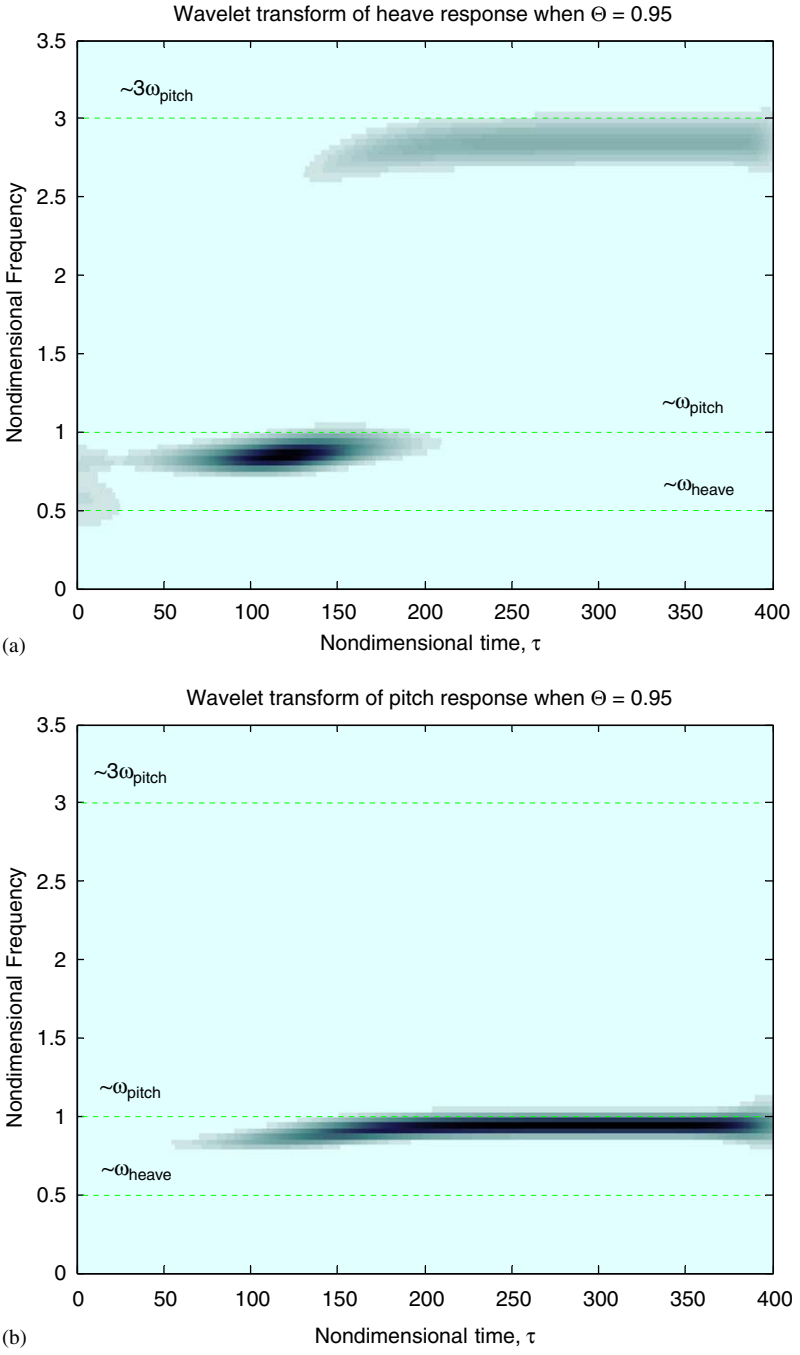

Fig. 6. Time-dependent frequency responses at a supercritical speed ($\Theta = 0.95$): (a) heave, and (b) pitch; initial conditions are $(y(0), \alpha(0), y'(0), \alpha'(0)) = (0.01, 0, 0, 0)$.

and $D = r_\alpha^2 - x_\alpha^2 > 0$ for any mass distribution. Note that only the coefficients $\zeta_1, \zeta_2, k_{12}, k_{22}$ are functions of the reduced velocity, Θ. Moreover, the condition $k_{12} \equiv 0$ resulting from the eigenvalue analysis determines the flutter speed,

$$\Theta_F \equiv \sqrt{\frac{r_\alpha^2 x_\alpha}{\mu C_{L,\alpha}(r_\alpha^2 + \gamma x_\alpha)}}, \tag{8}$$

so that, if $k_{12} < 0 \Rightarrow \Theta < \Theta_F$ and no flutter occurs.

Based on our previous finding that there exist at most three dominant frequency components in the subcritical and supercritical wind responses, we assume that the heave and pitch responses may be decomposed into three dominant frequency components, namely

$$y(\tau) = y_1(\tau) + y_2(\tau) + y_3(\tau),$$
$$\alpha(\tau) = \alpha_1(\tau) + \alpha_2(\tau) + \alpha_3(\tau). \tag{9}$$

The subscripts 1, 2, and 3 denote terms possessing three distinct dominant ('fast' in the terminology used in the following analysis) frequencies, i.e., being proportional to $e^{j\Omega\tau}, e^{j\tau}$, and $e^{3j\tau}$, respectively. Now, following Manevitch (2001) we introduce the following new complex variables:

$$\psi_1 = y_1' + j\Omega y_1, \quad \psi_3 = y_2' + jy_2, \quad \psi_5 = y_3' + 3jy_3,$$
$$\psi_2 = \alpha_1' + j\Omega\alpha_1, \quad \psi_4 = \alpha_2' + j\alpha_2, \quad \psi_6 = \alpha_3' + 3j\alpha_3, \tag{10}$$

where $j^2 = -1$.

Thus, denoting by ( )* the complex conjugate, we may express the original real variables in terms of the new complex ones:

$$y = \frac{1}{2j\Omega}(\psi_1 - \psi_1^*) + \frac{1}{2j}(\psi_3 - \psi_3^*) + \frac{1}{6j}(\psi_5 - \psi_5^*),$$
$$\alpha = \frac{1}{2j\Omega}(\psi_2 - \psi_2^*) + \frac{1}{2j}(\psi_4 - \psi_4^*) + \frac{1}{6j}(\psi_6 - \psi_6^*),$$
$$y' = \frac{1}{2}(\psi_1 + \psi_1^* + \psi_3 + \psi_3^* + \psi_5 + \psi_5^*),$$
$$\alpha' = \frac{1}{2}(\psi_2 + \psi_2^* + \psi_4 + \psi_4^* + \psi_6 + \psi_6^*),$$
$$y'' = \psi_1' + \psi_3' + \psi_5' - \frac{j\Omega}{2}(\psi_1 + \psi_1^*) - \frac{j}{2}(\psi_3 + \psi_3^*) - \frac{3j}{2}(\psi_5 + \psi_5^*),$$
$$\alpha'' = \psi_2' + \psi_4' + \psi_6' - \frac{j\Omega}{2}(\psi_2 + \psi_2^*) - \frac{j}{2}(\psi_4 + \psi_4^*) - \frac{3j}{2}(\psi_6 + \psi_6^*). \tag{11}$$

At this point we partition the complex responses into slow and fast parts:

$$\psi_1(\tau) = \varphi_1(\tau)e^{j\Omega\tau}, \quad \psi_3(\tau) = \varphi_3(\tau)e^{j\tau}, \quad \psi_5(\tau) = \varphi_5(\tau)e^{3j\tau},$$
$$\psi_2(\tau) = \varphi_2(\tau)e^{j\Omega\tau}, \quad \psi_4(\tau) = \varphi_4(\tau)e^{j\tau}, \quad \psi_6(\tau) = \varphi_6(\tau)e^{3j\tau}, \tag{12}$$

where $\varphi_k(\tau), k = 1, 2, \ldots, 6$ represent slowly varying complex-valued amplitude modulations. In expressing the variables according to (12) we assume that *the transient responses are composed of 'fast' oscillations* [represented by the complex exponentials in (12)] *modulated by 'slow' envelopes* [represented by the complex amplitudes $\varphi_k(\tau)$ *in* (12)]. This partition is fully compatible with the numerical simulations. It should be clear that the (slow) temporal evolution of the modulations $\varphi_k(\tau)$ govern the essential dynamics of system (6) in an appropriately defined slow-flow phase space. Interestingly enough, the dimensionality of the slow-flow phase space—in this case 12—differs from the dimensionality of the phase space of the original system (6)—which is 4; this is due to the fact that the dimensionality of the slow-flow phase space depends on the number of dominant harmonics that govern the transient dynamics—in this case 3.

Substituting (11) and (12) into (6) and applying the multiphase averaging (Lochak and Meunier, 1988) over the frequency components, $e^{j\Omega\tau}$, $e^{j\tau}$, and $e^{3j\tau}$, we obtain six complex-valued modulation equations of the form

$$\varphi' + F(\varphi; \Theta) = 0, F, \varphi \in \mathbb{C}^6, \Theta \in \mathbb{R}, \tag{13}$$

where the details of $F(\varphi; \Theta)$ can be found in the Appendix A.1, and the reduced velocity Θ is regarded as an independent parameter.

Figs. 7 and 8 show the validity of the averaged system with optimally determined initial conditions (see below) compared to the (numerically) exact solutions for both subcritical and supercritical reduced velocities. Our careful numerical study (not fully shown herein) indicates that the three-harmonic slow-flow model (13) approximates well the original dynamics at the entire range of reduced speeds, i.e., the averaged system is valid for accurately modeling the nonlinear dynamics over the entire subsonic fluid–structure interaction regime.

We note that each of the dominant harmonic components in the model (9) can be recovered from the averaged system (13), according to the expressions

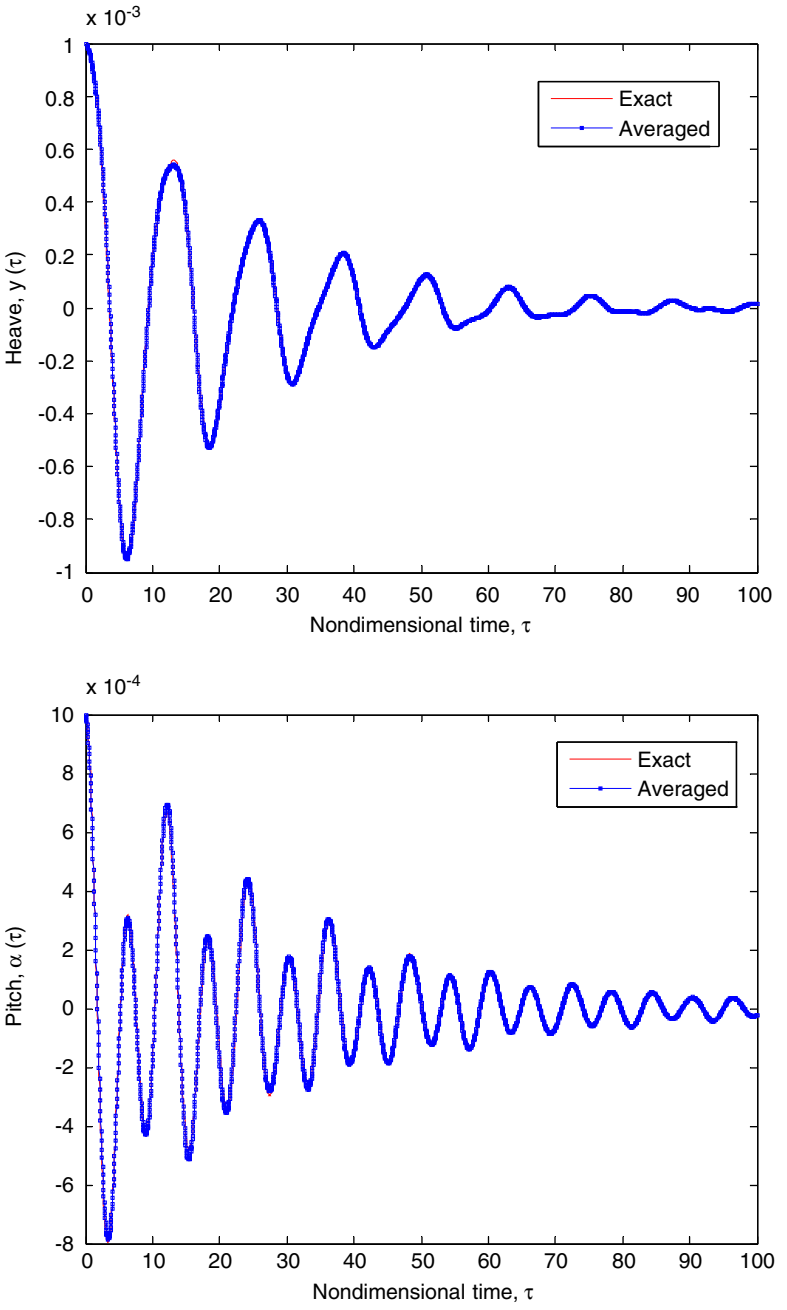

Fig. 7. Validation of the averaged system (13) for a subcritical reduced velocity ($\Theta = 0.5$); initial conditions are $(y(0), \alpha(0), y'(0), \alpha'(0)) = (10^{-3}, 10^{-3}, 0, 0)$.

$$
\begin{aligned}
y_1(\tau) &= \frac{1}{\Omega}\,\mathrm{Im}[\varphi_1(\tau)\mathrm{e}^{\mathrm{j}\Omega\tau}], \quad \alpha_1(\tau) = \frac{1}{\Omega}\,\mathrm{Im}[\varphi_2(\tau)\mathrm{e}^{\mathrm{j}\Omega\tau}],\\
y_2(\tau) &= \mathrm{Im}[\varphi_3(\tau)\mathrm{e}^{\mathrm{j}\tau}], \quad \alpha_2(\tau) = \mathrm{Im}[\varphi_4(\tau)\mathrm{e}^{\mathrm{j}\tau}],\\
y_3(\tau) &= \frac{1}{3}\,\mathrm{Im}[\varphi_5(\tau)\mathrm{e}^{3\mathrm{j}\tau}], \quad \alpha_3(\tau) = \frac{1}{3}\,\mathrm{Im}[\varphi_6(\tau)\mathrm{e}^{3\mathrm{j}\tau}],
\end{aligned}
\tag{14}
$$

so we may reconstruct the heave and pitch responses directly from the decompositions (9).

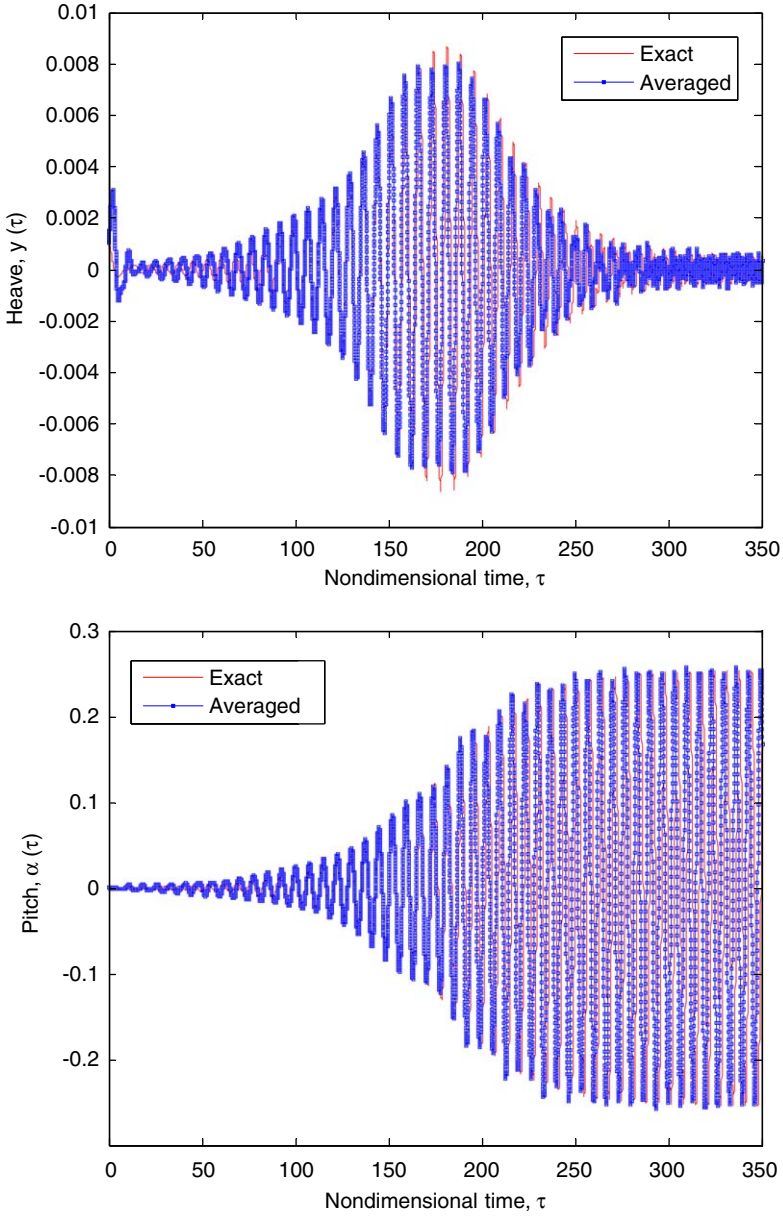

Fig. 8. Validation of the averaged system (13) for a supercritical reduced velocity ($\Theta = 0.95$); initial conditions are $(y(0), \alpha(0), y'(0), \alpha'(0)) = (10^{-3}, 10^{-3}, 0, 0)$.

An interesting point now discussed concerns the choice of initial conditions of the reduced set (13). Because we need twelve initial conditions for the averaged system (13), and we possess only four initial conditions for the full system (6), the problem or determining the appropriate initial conditions of the slow-flow model (13) becomes indeterminate. That is, we may write from the decomposition (9),

$$\begin{aligned} y(0) &= y_1(0) + y_2(0) + y_3(0), \quad \alpha(0) = \alpha_1(0) + \alpha_2(0) + \alpha_3(0), \\ y'(0) &= y_1'(0) + y_2'(0) + y_3'(0), \quad \alpha'(0) = \alpha_1'(0) + \alpha_2'(0) + \alpha_3'(0), \end{aligned} \tag{15}$$

which leads to the expressions,

$$\begin{aligned}
&\varphi_1(0) = y_1'(0) + \mathrm{j}\Omega y_1(0), \quad \varphi_2(0) = \alpha_1'(0) + \mathrm{j}\Omega\alpha_1(0),\\
&\varphi_3(0) = y_2'(0) + \mathrm{j}y_2(0), \quad \varphi_4(0) = \alpha_2'(0) + \mathrm{j}\alpha_2(0),\\
&\varphi_5(0) = y_3'(0) + 3\mathrm{j}y_3(0), \quad \varphi_6(0) = \alpha_3'(0) + 3\mathrm{j}\alpha_3(0),
\end{aligned} \tag{16}$$

under the restrictions:

$$\begin{aligned}
&\operatorname{Im}\varphi_3(0) = y(0) - [\Omega^{-1}\operatorname{Im}\varphi_1(0) + \tfrac{1}{3}\operatorname{Im}\varphi_5(0)],\\
&\operatorname{Im}\varphi_4(0) = \alpha(0) - [\Omega^{-1}\operatorname{Im}\varphi_2(0) + \tfrac{1}{3}\operatorname{Im}\varphi_6(0)],\\
&\operatorname{Re}\varphi_3(0) = y'(0) - [\operatorname{Re}\varphi_1(0) + \operatorname{Re}\varphi_5(0)],\\
&\operatorname{Re}\varphi_4(0) = \alpha'(0) - [\operatorname{Re}\varphi_2(0) + \operatorname{Re}\varphi_6(0)].
\end{aligned} \tag{17}$$

Determining the initial conditions for the averaged system (13) is thus converted to the following optimization problem:

$$\text{Compute}\left\{\min_{0<\tau\leqslant\hat{\tau}} \text{NMSE}(x(\tau), x_a(\tau))\right\}\text{for some } \hat{\tau}, \text{ subject to (17)}, \tag{18}$$

where the quantity to be minimized is regarded as function of the six sought initial conditions $\{\varphi_1(0), \ldots, \varphi_6(0)\}$, and NMSE stands for *normalized mean square error* and is defined as, $\text{NMSE} = E[||x - x_a||^2]/E[||x - E[x]||^2]$ where $E[\bullet]$ denotes the mean value and the standard inner product is used as the norm; moreover, $x(\tau) = (y(\tau), \alpha(\tau))$ and $x_a(\tau) = (y_a(\tau), \alpha_a(\tau))$ are the response vectors of the full and averaged systems, respectively. Note that the solution of the optimization problem (18) may not be unique, since it depends on the topological properties and singularities of the solution manifold in the corresponding space (for example, the solution manifold may have several local minima so that the 'optimal solution' can be computed as any one of them).

We may avoid this lack of uniqueness by expressing the solutions of (13) in Taylor series, $\varphi_i(\tau) = \sum_{j=0}^{N}\varphi_{ij}\tau^j + \mathcal{O}(\tau^{N+1})$ where $\varphi_{ij} \in \mathbb{C}, i = 1, \ldots, 6$ as $\tau \to 0$ (hence, we assume that $|\hat{\tau}| \ll 1$), and matching the series with the exact solutions at a specified matching instant of time to determine uniquely each of the Taylor coefficients. Then we can construct the normal equation and find the so-called Moore-Penrose least squares solution which should be unique in terms of the Fredholm Alternative Theorem [e.g., see Keener (2000)]. However, this kind of matching—in spite of uniqueness—may not provide good long-term results, particularly for higher-order approximations or multiphase averaging. For example, Keener (1977) studied the validity of the two-timing method (which is also called the method of multiple scales, or can be regarded as the first order averaging method) for limit cycles for large times; he showed that the approximate solution, which is *pointwise valid* only for times of order $\mathcal{O}(1/\varepsilon)$, is *orbitally valid* for large times in the sense that the approximate solution (although not pointwise valid for all times) approaches a valid approximation of a stable limit cycle.

Therefore, in this work we consider approximate solutions in the sense of orbital validity by way of the optimal initial conditions, instead of pointwise accuracy which is guaranteed only up to a small time scale and provides totally wrong prediction in the long run.

Considering the real-valued modulation equations of (13), two different formulations for analyzing the slow-flow dynamics can be followed, namely, further expressions of the complex quantities in Cartesian or polar coordinates. Let us first consider the slow-flow equations in Cartesian coordinates. Expressing $\varphi_k(\tau) = z_{2k-1}(\tau) + \mathrm{j}z_{2k}(\tau)$, $k = 1, \ldots, 6$, where $z_i \in \mathbb{R}$, $\forall i$ into (6), we obtain twelve (real-valued) slow-flow modulation equations:

$$Z' = G(Z;\Theta), \quad Z = (z_1, ..., z_{12}) \in \mathbb{R}^{12}, \quad \Theta \in \mathbb{R} \text{ (Cartesian coordinates)}. \tag{19}$$

Alternatively, expressing the complex quantities in polarform, we express $\varphi_k(\tau) = a_k(\tau)\mathrm{e}^{\mathrm{j}\beta_k(\tau)}$, $a_k \in \mathbb{R}^+, \beta_k \in S^1, k = 1, \ldots, 6$, which when substituted in (13), and upon separation of its real and imaginary parts, leads to a set of twelve equations of the form:

$$a_k' = \tilde{f}_k(a, \beta; \Theta) \quad \text{and} \quad a_k\beta_k' = \tilde{g}_k(a, \beta; \Theta).$$

The exact form of these equations is given in Appendix A.2. By combining these equations we derive the following autonomous set of alternative slow-flow modulation equations:

$$a_k' = f_k(a, \phi; \Theta), \quad a_i a_j \phi_{ij}' = g_n(a, \phi; \Theta) \text{ (polar coordinates)}, \tag{20}$$

where $k = 1, \ldots, 6$, and $(n; i, j) = (1; 1, 2), (2; 3, 5), (3; 3, 6), (4; 4, 5), (5; 4, 6)$. There are only five independent phase relations in (20) representing five phase differences between components of the solution with the following physical meanings:

- $\phi_{12} = \beta_1 - \beta_2$ represents the interaction between LF heave and LF pitch
- $\phi_{35} = 3\beta_3 - \beta_5$ represents the interaction between MF heave and HF heave
- $\phi_{36} = 3\beta_3 - \beta_6$ represents the interaction between MF heave and HF pitch
- $\phi_{45} = 3\beta_4 - \beta_5$ represents the interaction between MF pitch and HF heave
- $\phi_{46} = 3\beta_4 - \beta_6$ represents the interaction between MF pitch and HF pitch.

It can be shown that all other possible phase differences arising in (20) can be expressed in terms of these five independent phase variables; e.g., phase interaction between MF heave and MF pitch can be expressed as $\phi_{34} = \frac{1}{3}(\phi_{35} - \phi_{45})$ or $\frac{1}{3}(\phi_{36} - \phi_{46})$.

Although the modulation sets (19) and (20) are equivalent, in the following analysis we will be using the modulation equations in polar form, Eqs. (20), since they provide direct information on the amplitudes of the components of the solution, as well as, on the phases representing the nonlinear interactions between these components. A mathematical deficiency, however, of the equations in polar form relates to the mathematical singularity of the polar transformation at the origin, which renders the set (20) invalid for analyzing the dynamics when some or all of the components have zero (or nearly zero) amplitudes. In that case the modulation equations in Cartesian form, (19), should be used.

3.3. Steady-state dynamics

Before we utilize the slow-flow model (20) to study LCO triggering mechanism, we perform first a steady-state bifurcation analysis of the dynamics utilizing MATCONT, the numerical continuation code in Matlab® (Dhooge et al., 2003), in conjunction with the algorithm introduced in Kubíček (1976) utilizing parameterization with respect to the arc length of equilibrium loci.

To this end, we consider the original equations of motion (6), and express them in the first order form

$$x' = X(x; \Theta) \quad \text{where } x = (y, \alpha, y', \alpha') \in \mathbb{R}^4, \quad \Theta \in \mathbb{R}.$$

Direct application of MATCONT on these first order differential equations gives bifurcation diagrams that provide global information on the dynamics of the full system at steady state (Fig. 9). As we discussed in Section 2, the (stable) trivial equilibrium $x = 0$ undergoes a Hopf bifurcation at the flutter speed at $\Theta_F = 0.87$, and changes its stability with simultaneous generation of a stable LCO. When the reduced velocity reaches the divergence flutter speed $\Theta_D = 1.767$, two unstable nontrivial equilibrium points are computed. The solution curve for heave appears almost vertical at Θ_D, while that for pitch does not. The physical interpretation is that, for reduced velocities higher than the divergence flutter speed, almost every heave position can be an equilibrium point whereas the pitch mode possesses a specific equilibrium position. We note that, if we zoom out the vertical axis in Fig. 9(a) to the same order as in Fig. 9(b), then the heave equilibrium curve also looks like a parabola; but this understanding may not be physically meaningful. In any case, these nontrivial equilibrium points are unstable so that they are not physically realizable.

The divergence flutter represents a static instability (Blevins, 1990) and the corresponding reduced speed can be computed from static balance as

$$\Theta_D \equiv \sqrt{r_\alpha^2/(\gamma \mu C_{L,\alpha})}. \tag{21}$$

Since the above results provide only global information regarding to where and what type of bifurcations occur, and how large the LCO amplitudes are, they will not help us understand the modal interactions that generate the fluid–structure instabilities and eventually act as LCO triggering mechanisms. Therefore, we perform bifurcation analysis for the averaged system (19) for the trivial equilibrium via MATCONT, and for (20) for the nontrivial LCOs utilizing Kubíček's method (1976). The reason for using two different approaches is dictated by the possible singularities built in (20); e.g., if one of the amplitudes becomes zero, then the equations become singular (i.e., it degenerates to a set of differential-algebraic equations) and becomes unsolvable using MATCONT (which only solves differential equations of the standard form $x' = X(x; \sigma)$ where $x \in \mathbb{R}^n, \sigma \in \mathbb{R}^k$).

Fig. 10 depicts the numerical continuation results for steady-state amplitudes and phase differences for the multiphase averaged system (20) (recall the optimization problem for determining the initial conditions in Section 3.2, and note that these solutions may not be unique.) We can clearly see that after the flutter speed the HF heave and MF pitch components are dominant at steady state, which is exactly consistent with the numerical simulations. These

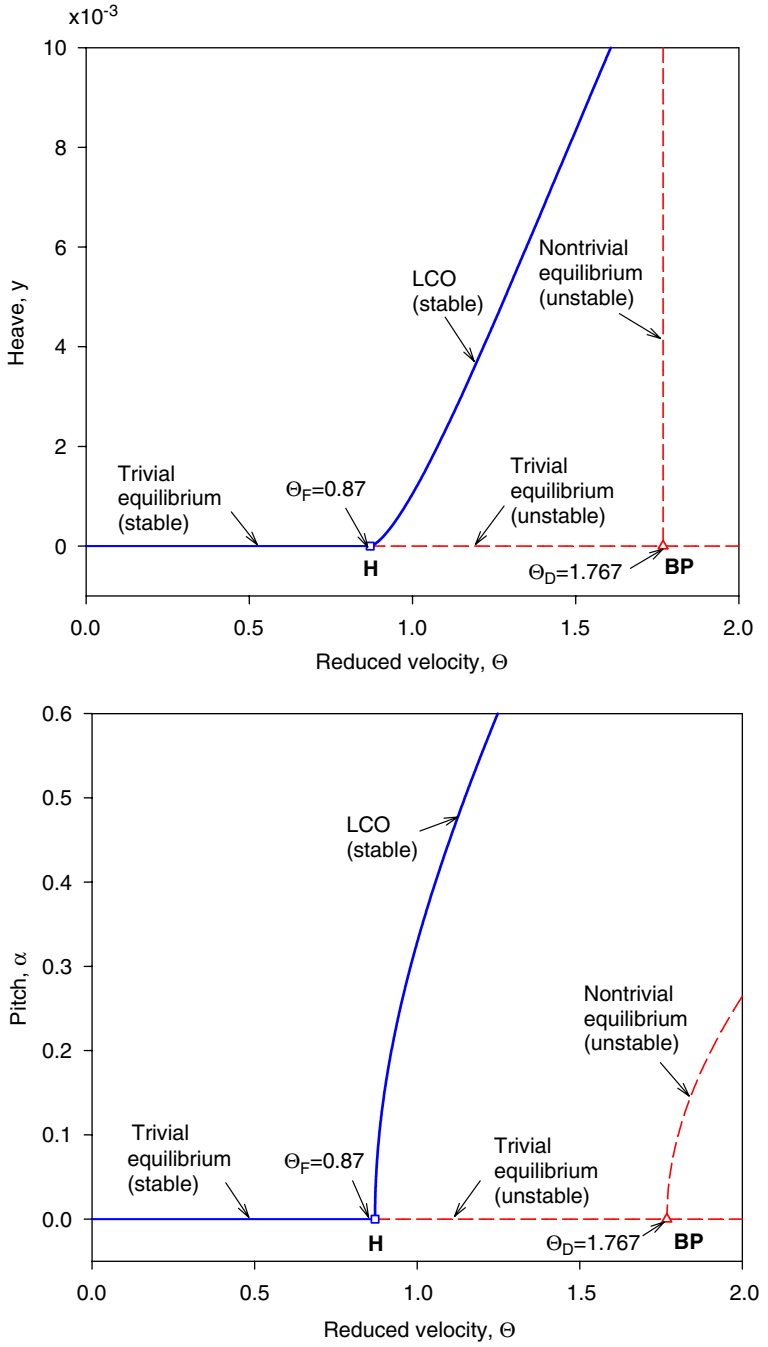

Fig. 9. Bifurcation analysis of the trivial equilibrium directly from the equations of motion (6); 'H' and 'BP' stand for Hopf bifurcation point and branching point, respectively; stable (unstable) motion is represented by a solid (dashed) line.

steady-state results will be revisited in Section 4.3, where analytical study of the LCO triggering mechanism is carried out.

Because our wing model assumes small oscillations, $|\alpha| < 10^\circ \approx 0.1745$ radians, the numerical solutions at higher supercritical speeds may deviate from physical observations. In addition, we may not observe the secondary Hopf

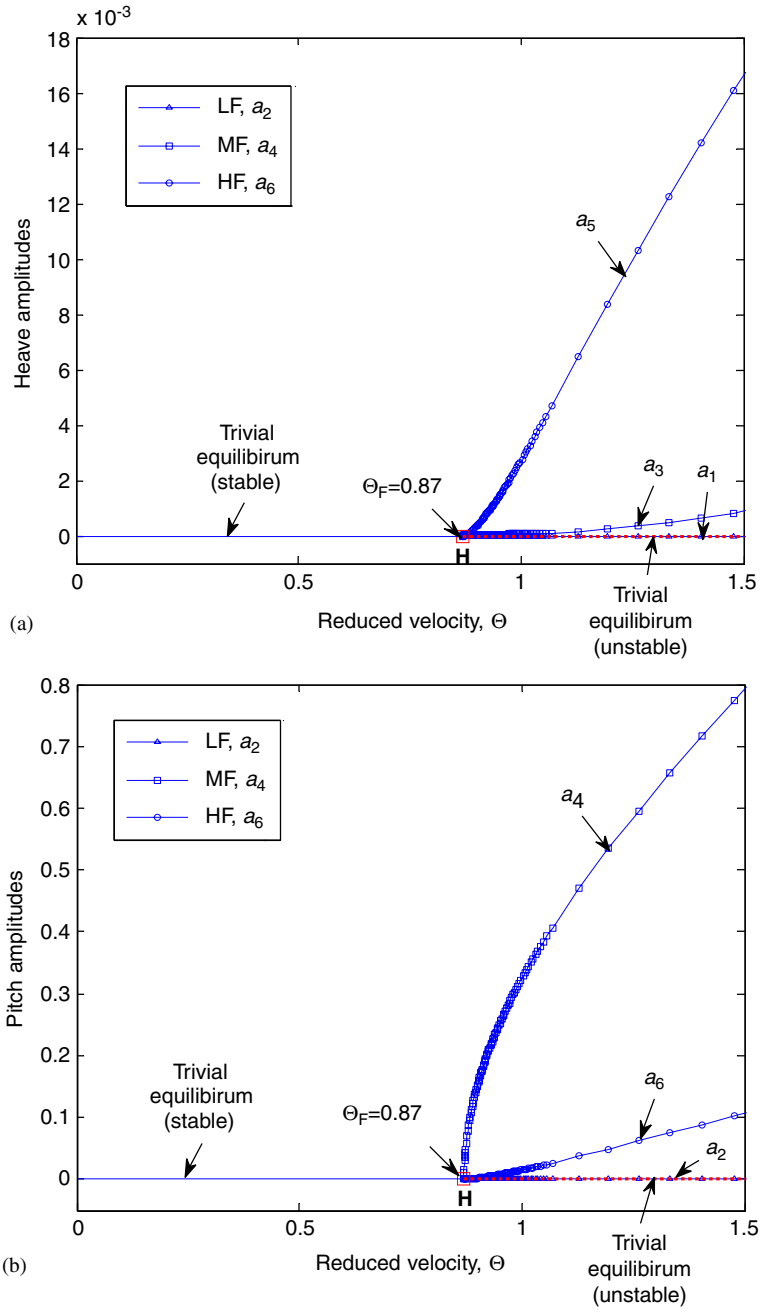

Fig. 10. Steady-state LCO amplitudes and phase differences from the averaged system (15, 16); (a) heave amplitudes, (b) pitch amplitudes, (c) and (d) phase differences.

bifurcation by our slow-flow analysis since at least five dominant harmonics are required for it (Liu and Dowell, 2004). Moreover, only supercritical LCOs will be obtained due to the specific parameter choices.

We now examine the possible existence of other equilibrium solutions of the slow-flow Eqs. (20). In fact, there exist many other nontrivial but degenerate equilibrium solutions; Fig. 11 presents one of those computed by numerical continuation of equilibria, i.e., all near-trivial amplitudes except the LF pitch, a_2, and corresponding phase-difference relations. The LF pitch amplitude a_2 in Fig. 11(a) is equal to $\Omega a_4 = 0.5a_4$, where a_4 is the MF pitch amplitude in Fig. 10(b); although it can be obtained analytically below, we may intuitively guess the relation by examining the

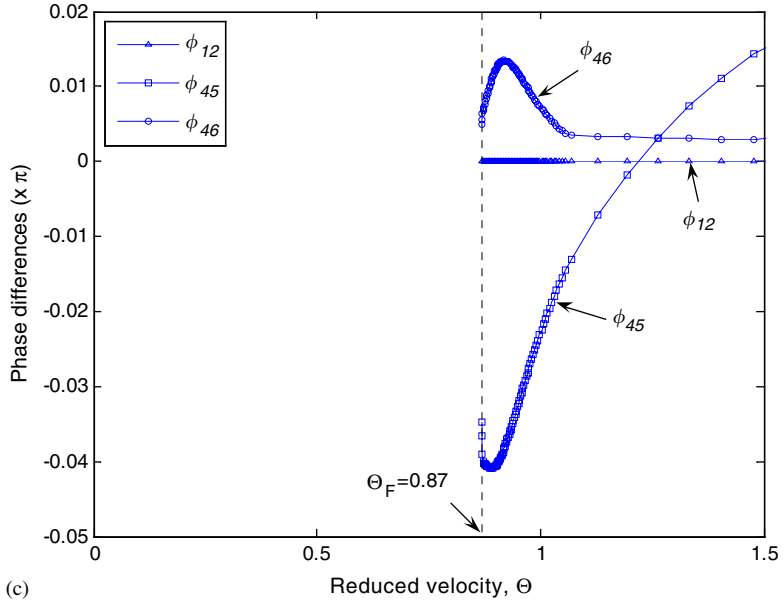

(c)

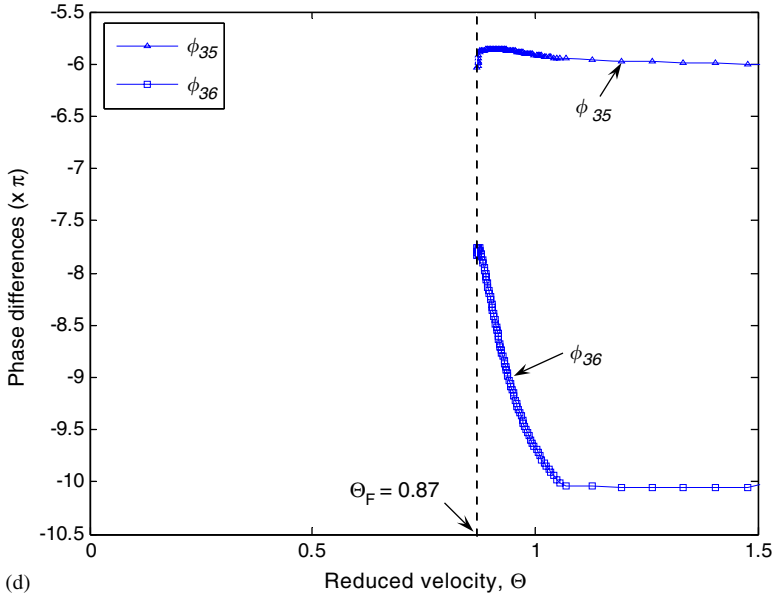

(d)

Fig. 10. (*Continued*)

expression of the amplitudes in (14) and considering a specific balanced energy value for a specific reduced speed. For example, suppose that we have a certain balanced energy level for $\Theta = 0.95$, all the amplitudes except LF or MF pitch are almost trivial, and that we know the LCO amplitude in pitch as $\alpha = 0.2525$ (note that in general the contribution of heave mode to the total energy at steady state is quite negligible; see, for example, Fig. 17(b)). Then, $\alpha = a_4$ when only MF pitch is dominant; if only LF pitch is dominant, then we may compute $\alpha = a_2/\Omega = a_4$ by (14).

Figs. 12 and 13 show heave and pitch responses that correspond to the steady state motions at $\Theta = 0.95$ depicted in Figs. 10 and 11, respectively. In both cases, the same initial conditions are used: $(y(0), \alpha(0), y'(0), \alpha'(0)) = (10^{-3}, 10^{-3}, 0, 0)$. However, those for the slow-flow Eqs. (20) are different; i.e., initial conditions for Fig. 12 are optimal ones to accurately approximate the exact solutions which will be used later in the study of LCO triggering mechanism, whereas those for Fig. 13 are slightly different. Since the numerical observation can be made only for stable motions, both steady-state solutions found in Figs. 10 and 11 are stable ones, but it turns out the prediction depicted in

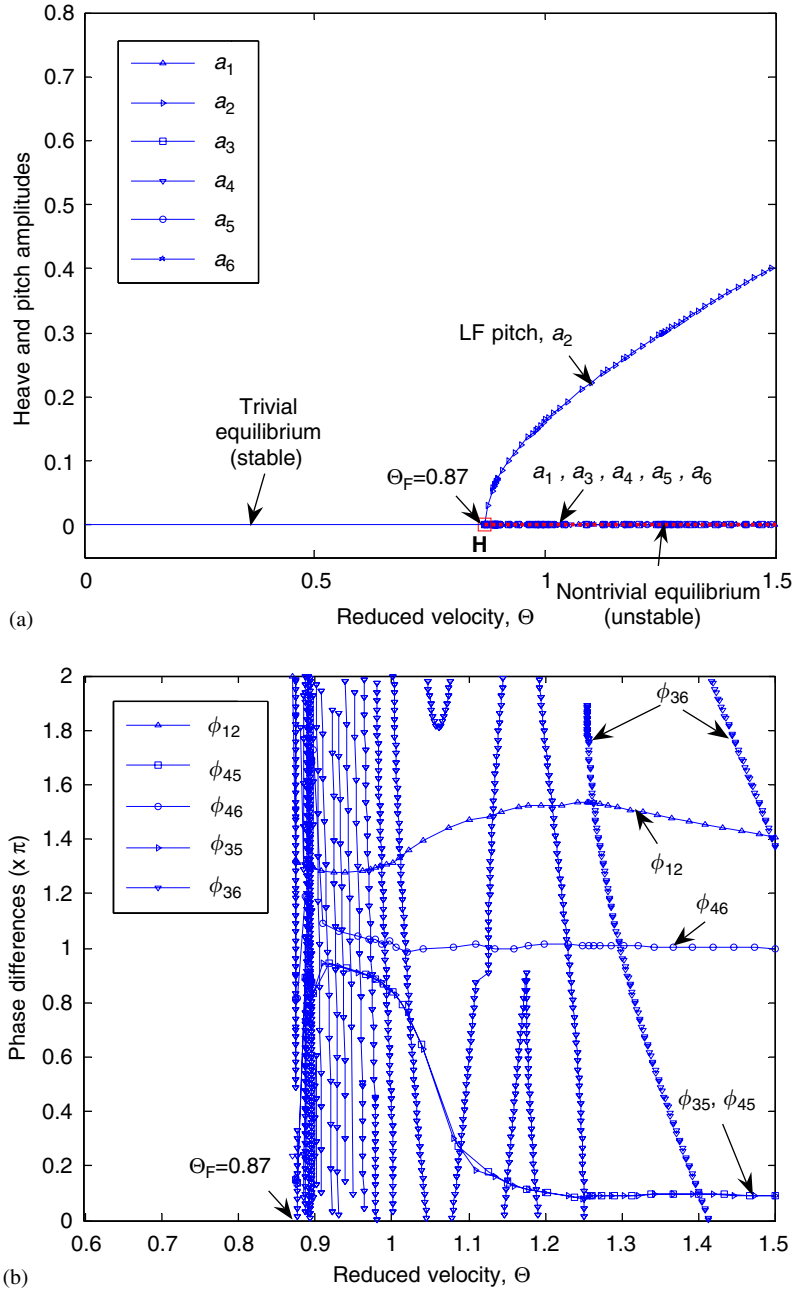

Fig. 11. Another steady-state LCO amplitudes and phase differences from the averaged system (15, 16); (a) amplitudes, (b) phase differences (note that mod 2π was applied for the plot of ϕ_{36}).

Fig. 13 is not meaningful in our study of the LCO triggering mechanism because it is based on a degenerate equilibrium of the slow-flow modulation equations, and does not provide any information on the HF heave component which is observable in reality.

The degenerate equilibrium solutions presented in Fig. 11 can be derived analytically from a subsystem of slow-flow model (20), i.e., from the multiphase averaged system with two dominant frequencies corresponding to LF and MF components—it will be called the two-frequency averaged system hereafter. For this subsystem, we neglect HF terms of $y_3(\tau)$ and $\alpha_3(\tau)$ in (9) which are the decomposition corresponding to HF components; or get rid of the complex variables

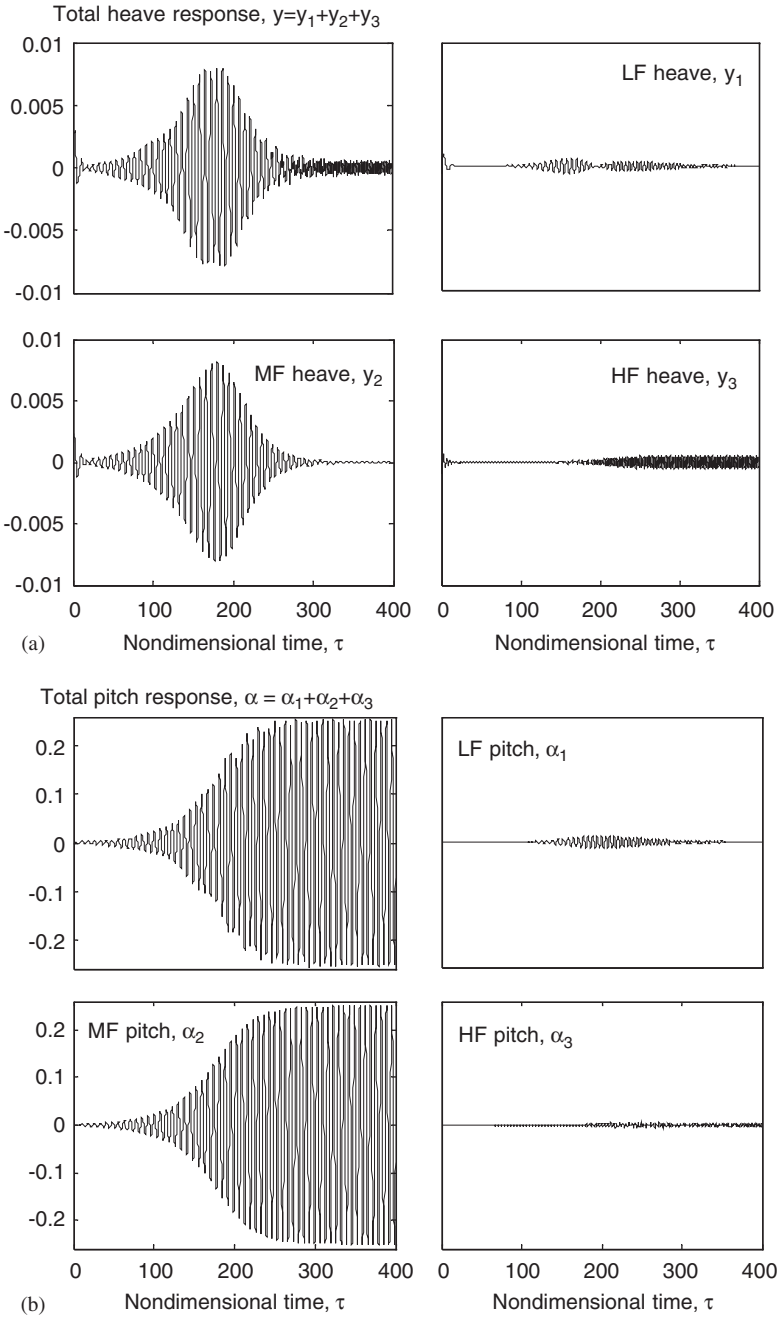

Fig. 12. Total and each component responses whose steady-state solutions correspond to those in Fig. 10 when $\Theta = 0.95$: (a) heave and (b) pitch.

of ψ_5 and ψ_6 introduced in (10)–(12) so that the resulting complex-valued slow-flow equation (13) retain only $\varphi_1, \ldots, \varphi_4 \in \mathbb{C}$. Then, from Appendix A.2, we obtain a reduced two-frequency averaged system in polar form,

$$a_1' + \frac{\zeta_1}{2} a_1 - \frac{a_2}{2\Omega} \sin\,\phi_{12} \left(k_{12} + \frac{3n_{12}}{4\Omega^2} a_2^2 + \frac{3n_{12}}{2} a_4^2 \right) = 0, \tag{22a}$$

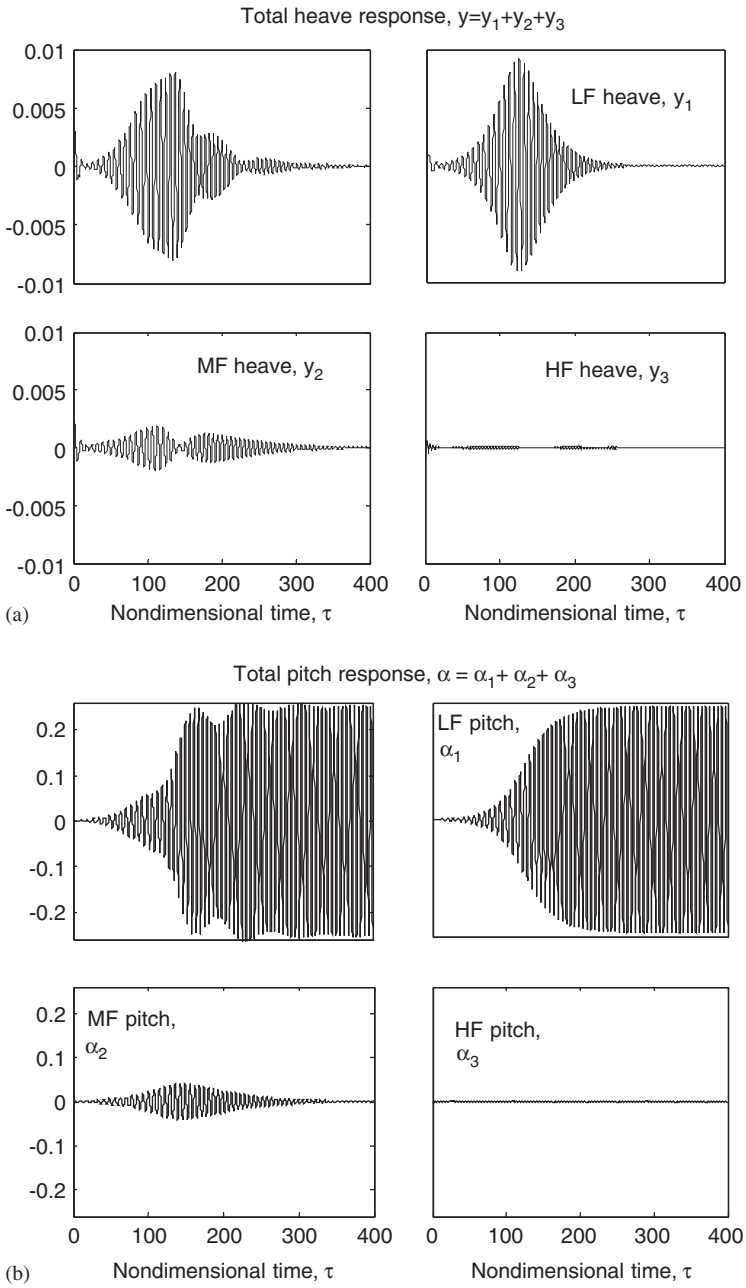

Fig. 13. Total and each component responses whose steady-state solutions correspond to those in Fig. 11 when $\Theta = 0.95$: (a) heave, (b) pitch, (c) and (d) phase differences.

$$a_2' + \frac{\zeta_2}{2} a_1 \cos\phi_{12} + \frac{a_1}{2\Omega} \sin\phi_{12} \left(k_{21} + \frac{3n_{21}}{4\Omega^2} a_1^2 + \frac{3n_{21}}{2} a_3^2 \right) = 0, \tag{22b}$$

$$a_3' + \frac{\zeta_1}{2} a_3 - \frac{a_4}{2} \sin\phi_{34} \left(k_{12} + \frac{3n_{12}}{2\Omega^2} a_2^2 + \frac{3n_{12}}{4} a_4^2 \right) = 0, \tag{22c}$$

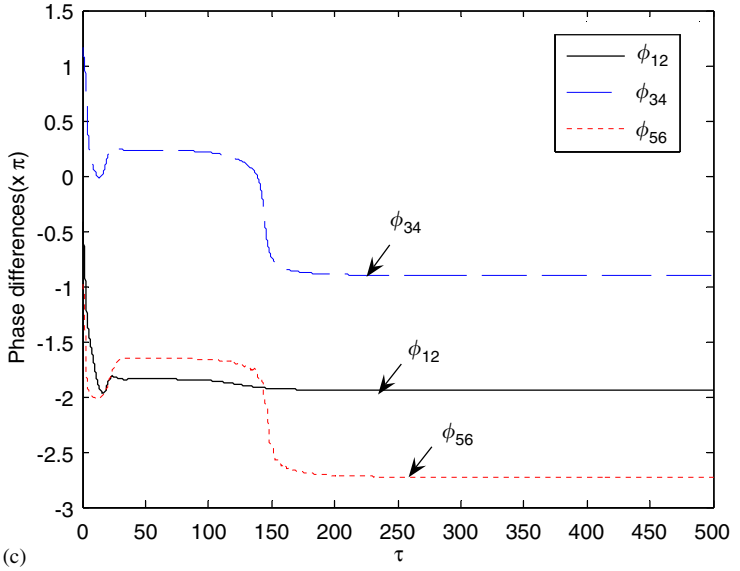

(c)

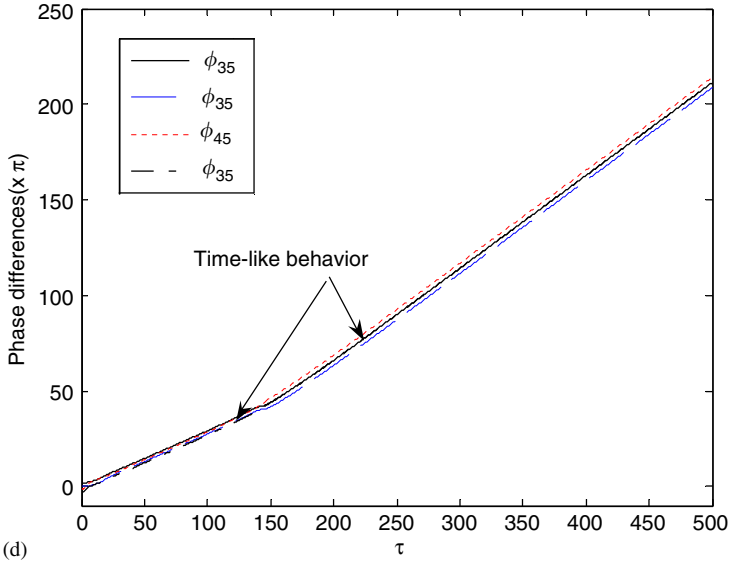

(d)

Fig. 13. (*Continued*)

$$a_4' + \frac{\zeta_2}{2} a_3 \cos\phi_{34} + \frac{a_3}{2} \sin\phi_{34} \left(k_{21} + \frac{3n_{21}}{2\Omega^2} a_1^2 + \frac{3n_{21}}{4} a_3^2 \right) = 0, \tag{22d}$$

$$a_1 a_2 \phi_{12}' + \frac{a_1 a_2}{2\Omega} \left(k_{22} - k_{11} - \frac{3n_{11}}{4\Omega^2} a_1^2 - \frac{3n_{11}}{2} a_3^2 + \frac{3n_{22}}{4\Omega^2} a_2^2 + \frac{3n_{22}}{2} a_4^2 \right) - \frac{\zeta_1}{2} a_1^2 \sin\phi_{12}$$
$$- \frac{1}{2\Omega} \cos\phi_{12} \left[a_2^2 \left(k_{12} + \frac{3n_{12}}{4\Omega^2} a_2^2 + \frac{3n_{12}}{2} a_4^2 \right) - a_1^2 \left(k_{21} + \frac{3n_{21}}{4\Omega^2} a_1^2 + \frac{3n_{21}}{2} a_3^2 \right) \right] = 0, \tag{22e}$$

$$a_3 a_4 \phi_{34}' + \frac{a_3 a_4}{2} \left(k_{22} - k_{11} - \frac{3n_{11}}{2\Omega^2} a_1^2 - \frac{3n_{11}}{4} a_3^2 + \frac{3n_{22}}{2\Omega^2} a_2^2 + \frac{3n_{22}}{4} a_4^2 \right) - \frac{\zeta_2}{2} a_3^2 \sin\phi_{34}$$
$$- \frac{1}{2} \cos\phi_{34} \left[a_4^2 \left(k_{12} + \frac{3n_{12}}{2\Omega^2} a_2^2 + \frac{3n_{12}}{4} a_4^2 \right) - a_3^2 \left(k_{21} + \frac{3n_{21}}{2\Omega^2} a_1^2 + \frac{3n_{21}}{4} a_3^2 \right) \right] = 0, \tag{22f}$$

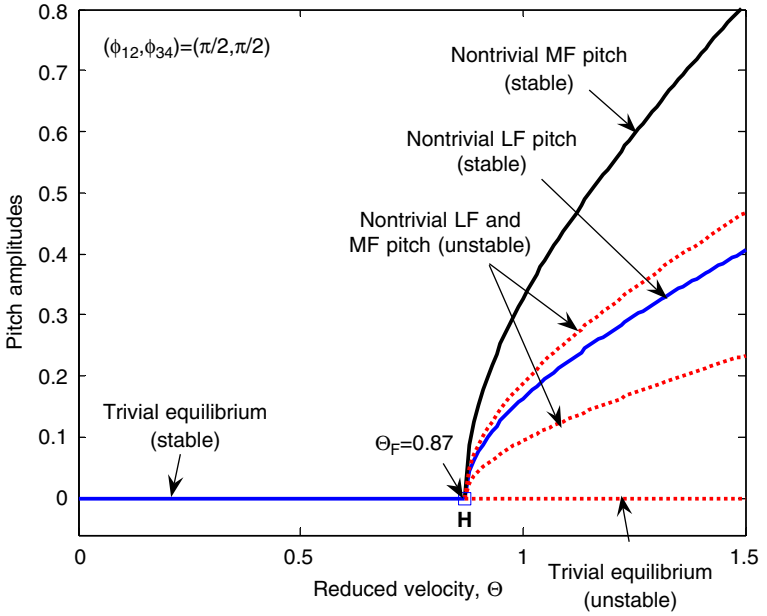

Fig. 14. Analytical steady-state pitch amplitudes with stability when $(\phi_{12}, \phi_{34}) = (\pi/2, \pi/2)$ and are computed from the two-frequency averaged system (22).

where in this case there appear only two likewise phase relations, i.e., phase interaction between LF heave and LF pitch modes, $\phi_{12} = \beta_1 - \beta_2$, and that between MF heave and MF pitch modes, $\phi_{34} = \beta_3 - \beta_4$.

For steady-state solutions, we set $a_1' = \cdots = a_4' = \phi_{12}' = \phi_{34}' = 0$ in (22), and obtain a set of six algebraic equations, from which the equilibrium solutions can be computed. First we consider the case where $(\phi_{12}, \phi_{34}) = (m\pi, n\pi)$ and $m, n \in \mathbb{N}$, and substitute $\sin\phi_{12} = \sin\phi_{34} \equiv 0$, $\cos\phi_{12} = \cos\phi_{34} \equiv \pm 1$ into (22) to obtain $a_1 = a_3 = 0$ from (22a) to (22d), i.e., only trivial solutions for heave mode. Then, (22e) and (22f) yield two conditions:

$$a_2^2\left(k_{12} + \frac{3n_{12}}{4\Omega^2}a_2^2 + \frac{3n_{12}}{2}a_4^2\right) = 0 \quad \text{and} \quad a_4^2\left(k_{12} + \frac{3n_{12}}{2\Omega^2}a_2^2 + \frac{3n_{12}}{4}a_4^2\right) = 0. \tag{23}$$

The solutions for (23) are the following four cases:

(i) $a_2 = a_4 \equiv 0$: Trivial solutions (24a)

(ii) $a_4 \equiv 0$ but $a_2 \neq 0$: Nontrivial LF pitch mode,
i.e., $a_2 = 2\Omega\sqrt{-k_{12}/(3n_{12})}$ if $k_{12}/n_{12} < 0$ (24b)

(iii) $a_2 \equiv 0$ but $a_4 \neq 0$: Nontrivial MF pitch mode,
i.e., $a_4 = 2\sqrt{-k_{12}/(3n_{12})}$ if $k_{12}/n_{12} < 0$ (or $\Theta > \Theta_F$) (24c)

(iv) $a_2 \neq 0$ and $a_4 \neq 0$: Nontrivial LF and MF pitch modes,
i.e., $a_2 = \frac{2}{3}\Omega\sqrt{-k_{12}/n_{12}}$, $a_4 = \frac{2}{3}\sqrt{-k_{12}/n_{12}}$ if $k_{12}/n_{12} < 0$. (24d)

Similarly, for combinations of phase differences $(\phi_{12}, \phi_{34}) = (m\pi, (2n+1)\pi/2)$, $((2m+1)\pi/2, n\pi)$, and $((2m+1)\pi/2, (2n+1)\pi/2)$ where $m, n \in N$, we can also compute the same equilibrium solutions as in (24). Furthermore, we can evaluate their stability analytically, although the perturbed equations become a set of differential-algebraic equations due to the singular amplitudes; the two resulting algebraic equations from (22e,f) act as constraints to the four first-order differential modulation equations so that we can evaluate the eigenvalues of the (4×4) Jacobian matrix evaluated at the equilibrium to determine its stability; in some cases we come up with zero eigenvalues, and higher-order perturbation techniques may be required to evaluate stability. Detailed evaluation of the stability will not be discussed

in this study. It is, however, remarked that the stability of equilibrium solutions depends on phase relations. Fig. 14 depicts one specific set of steady-state amplitudes when $(\phi_{12}, \phi_{34}) = (\pi/2, \pi/2)$; these steady-state solutions for the two-frequency averaged system can be regarded as a degenerate subset of the three-frequency averaged system (13).

In Fig. 15, we present special orbits in the phase space projected onto LF heave versus LF pitch, and MF heave versus MF pitch planes when $\Theta = 1.1$; they are completed starting from the set of initial conditions lying on the stable and unstable eigenvectors evaluated at each equilibrium point by forward and backward integrations. Due to the high dimensionality of the phase space, one may hardly conclude that those orbits are homoclinic or heteroclinic orbits. Nonetheless, those special orbits give some insights regarding the LCO triggering mechanism. That is, given an initial state close to the trivial equilibrium, it will be thrown away from the initial state due to the instability at the trivial equilibrium (transient regime); the dynamics will approach and stay for some period close to one of the equilibrium position possessing both stable and unstable manifolds (denoted TRC at Stage I; see Section 4.1 for the definition); it will slowly escape from near the unstable equilibrium (Escape at Stage II) then permanently captured to the final stable

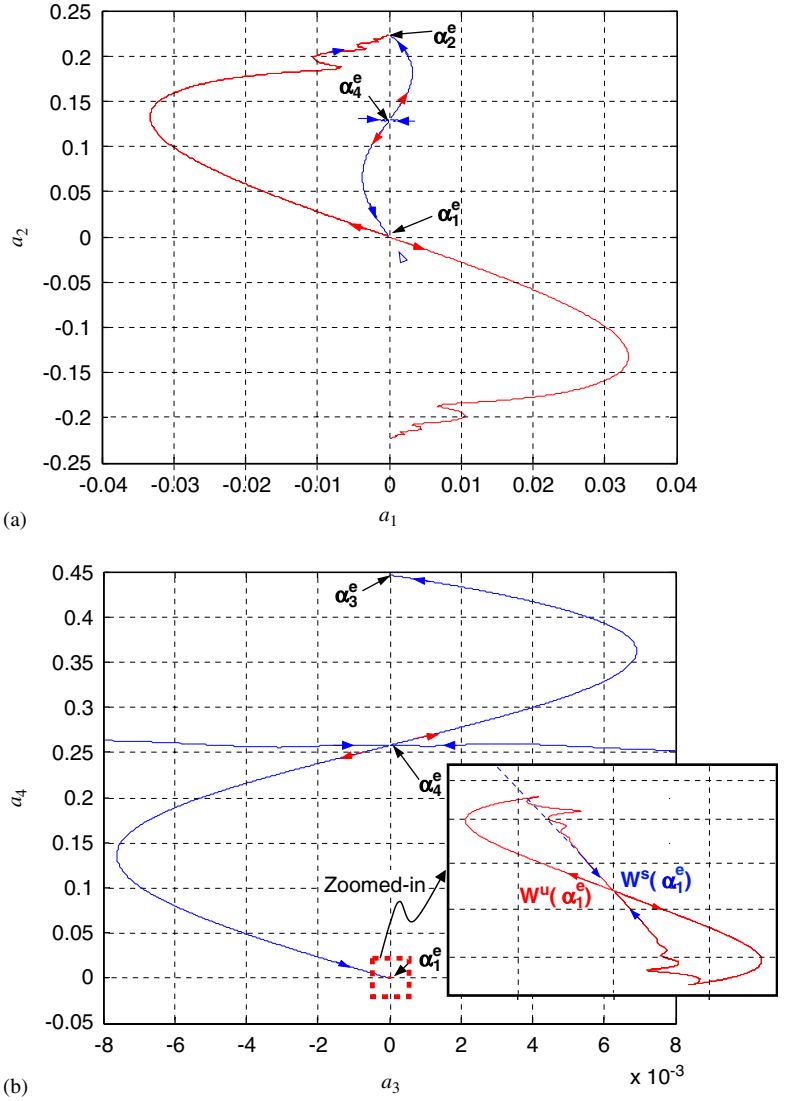

Fig. 15. Special orbits in the phase space projected onto (a) LF heave vs. LF pitch, and (b) MF heave vs. MF pitch planes when $\Theta = 1.1$; they are computed with the set of initial conditions lying on the stable and unstable eigenvectors evaluated at each equilibrium point by forward and backward integrations; by $\alpha_1^e, \ldots, \alpha_4^e$ we denote the equilibrium amplitudes determined by (24a–d) in sequence; and W^S (W^U) are the stable (unstable) manifolds at the corresponding equilibrium.

equilibrium position (PRC at Stage III). This description makes sense by examining Fig. 13(c) where we may say roughly the time interval $[0, 30]$ corresponds to transient regime; $[30, 100]$ to TRC; $[100, 200]$ to escape; and finally $[200, \tau \gg 1)$ to PRC. These apparent resonance captures only refer to those valid in the degenerated phase space. The LCO triggering mechanism will be explored both numerically and analytically in Sections 4.2 and 4.3.

4. LCO triggering mechanisms

In this section, we show numerically and analytically that resonance captures are responsible for the triggering and developing LCOs. For this purpose, we first introduce some definitions such as transient and permanent capture, escape, and passage through resonance; and we review the concepts of internal resonance and resonance capture.

4.1. Definitions

Resonance capture (or capture/entrapment into a resonance manifold) can be regarded as a form of transient internal resonance, whereby an orbit of the dynamical system is captured in the neighborhood of a resonance manifold in phase space, triggering vigorous energy exchanges between different subsystems. Moreover, resonance captures prevent the direct application of the averaging principle particularly in systems with multiple frequencies (Arnold, 1988; Sanders and Verhulst, 1985); on the other hand, resonance captures lead to interesting energy exchanges and dynamic interactions in celestial mechanics, orbital mechanics, or even in particle dynamics (Koon et al., 2001; Belokonov and Zabolotnov, 2002; Itin et al., 2000), and is also a very important dynamic behavior in studying the so-called *nonlinear energy pumping phenomenon*, which makes possible irreversible and one-way, passive energy transfer from one component of a dynamical system to a different component, which acts, in essence, as a nonlinear energy sink (Vakakis and Gendelman, 2001; Vakakis et al., 2003; Kerschen et al., 2006).

Definition (Sanders and Verhulst, 1985): Consider the system in polar form with multiphase angles

$$r' = \varepsilon R(\phi, r), \quad \phi' = \Omega(r), \tag{25}$$

where $r \in \mathbb{R}^p$, $\phi \in T^q$ (generally, $q \leqslant p$), $\Omega(r) = (\Omega_1(r), \Omega_2(r), \ldots, \Omega_q(r))$, and the dimension of r may be greater than that of the original dynamical system, depending on frequency decompositions [this is indeed the case in this work—compare Eqs. (2) and (20)]. The set of points in $D \subset \mathbb{R}^p$ where $\Omega_i(r) \equiv 0$, $i = 1, 2, \ldots, q$ is called the *resonance manifold*. This resonance condition is *not sufficient*; that is, if each $\Omega_i(r)$, $i = 1, 2, \ldots, q$ is away from zero, the *internal resonance manifold* is defined as the set $\{r \in \mathbb{R}^p : \langle k, \Omega(r) \rangle = 0,\ k \in \mathbb{Z}^q\}$ where the corresponding Fourier coefficients from $R(\phi, r)$ are not identically zero.

Assume that the averaged system intersects transversely the resonant manifold. Roughly, capture into resonance may occur for some phase relations satisfying the condition that an orbit of the dynamical system reaching the neighborhood of the resonant manifold continues in such a way that the commensurable frequency relation is approximately preserved; in this situation not all phase angles are fast (time-like) variables, so classical averaging cannot be performed with regard to these angles. As a result, over the time scale $1/\varepsilon$ the exact and averaged solutions diverge up to $\mathcal{O}(1)$ (Arnold, 1988).

Definition (Bosley and Kevorkian, 1992): Suppose that (internal) resonance occurs at a time instant $t = t_0$, with the nontrivial frequency combination $\sigma = k_1\omega_1 + k_2\omega_2 + \cdots + k_q\omega_q$, where $k_i \in \mathbb{Z}$, $i = 1, \ldots, q$, vanishing at that time instant $t = t_0$. Then, *sustained resonance* is defined to occur when $\sigma \approx 0$ persists for times $t - t_0 = \mathcal{O}(1)$. On the other hand, *transient resonance* refers to the case when σ makes a single slow passage through zero.

Definition (Quinn, 1997a): The possible behavior of trajectories near the resonance manifold on the time scale $1/\varepsilon$ is described according to the following three cases: (i) *Capture*: Solutions are unbounded in backward time. However, captured trajectories remain bounded for forward times of $\mathcal{O}(1/\varepsilon)$, i.e., a sustained resonance exists in forward time; (ii) *Escape*: Solutions grow unbounded in forward time. However, in backward time, solutions remain bounded for times of $\mathcal{O}(1/\varepsilon)$, i.e., a sustained resonance exists in backward time; and (iii) *Pass-through*: Solutions do not remain in the neighborhood of the resonance manifold in either forward or backward time. No sustained resonance exists.

A mechanism for resonance capture in perturbed two-frequency Hamiltonian systems was studied by Burns and Jones (1993) where the most probable mechanisms for resonance capture are described to involve an interaction

between the asymptotic structures of the averaged system and a resonance. It was shown that, if the system satisfies a less restrictive condition [or Condition N (Lochak and Meunier, 1988)] regarding transversal intersection of the averaged orbits to the resonance manifold, resonance capture can be viewed as an event with low probability, and passage through resonance is the typical behavior on the time scale $1/\varepsilon$.

Necessary conditions were proved in Kath (1983a) both for entrainment to sustained resonance and for its continuance (and thus the possible indication of unlocking or escape from the sustained resonance after a finite time) by successive near-identity transformations; a sufficient condition was also derived for continuation of sustained resonance by means of matched asymptotic expansions (Kath, 1983b).

On the other hand, transition to escape was studied by Quinn (1997b) in a coupled Hamiltonian system consisting of two identical oscillators possessing a homoclinic orbit when uncoupled. Focusing on intermediate energy levels at which sustained resonant motion occurs, he analyzed the existence and behavior of those motions in equipotential surfaces whose trajectories are shown to remain in the transiently stochastic region for long times and, finally, to escape or leak out of the opening in the equipotential curves and proceeding to infinity.

Regarding passage through resonance, one may refer to, for example, Neishtadt (1975). The phenomenon of passage-through resonance is sometimes referred to as nonstationary resonances caused by excitations having time-dependent frequencies and amplitudes (Nayfeh and Mook, 1979).

Finally, we conclude this section with the following alternative definitions which are useful for understanding LCO triggering mechanisms when multifrequency components are considered.

Definition (Burns and Jones, 1993): Consider an unforced n-dof system whose linear natural frequencies are ω_k, $k = 1, \ldots, n$. We define (i) *Internal Resonance* (IR) as motions for which there exist $k_i \in \mathbb{Z}$, $i = 1, 2, \ldots, n$, such that $k_1\omega_1 + \cdots + k_n\omega_n \approx 0$, i.e., some combination of linear natural frequencies satisfy commensurability; (ii) *Transient Resonance Capture* (TRC) as capture into a resonance manifold which occurs and continues for a certain period of time (for example, on the time scale $1/\varepsilon$) and then finally involves transition to escape. This includes sustained resonance captures involving escape; and (iii) *Permanent Resonance Capture* (PRC) as sustained resonance captures that will never escape for increasing time.

It was also noted that the PRC is quite likely for the pendulum-like equations (or called pendulum normal form) obtained by a partial averaging in the neighborhood of a given resonance in the original dynamics which can have infinitely many resonances. Unstable equilibrium point of the corresponding unperturbed pendulum system should be nondegenerate by Neishtadt's Condition B (Arnold, 1988), which is another weaker transversality condition; for example, a single dof pendulum equation possesses an unstable equilibrium point (i.e., a saddle point) when the mass is vertically upward, and there exist a homoclinic orbit passing the saddle point and enclosing a stable equilibrium which indicates the vertically-downward position. Accordingly, the behavior of PRCs were formulated in two theorems: one is regarding existence of an attractor near the resonance manifold; the other, for its domain of attraction and hence the likelihood of resonance captures tending asymptotically to the resonant attractor (Burns and Jones, 1993).

Both TRC and PRC may occur along the internal resonance manifold, and are distinguished by whether they involve an escape or not. Both IR and PRC may show similar steady-state behaviors, which differ from the commensurability condition between linear natural frequencies. Hereafter when we mention a $m:n$ internal resonance, it refers to a condition on the slow-flow averaged system unless otherwise noted.

For more details on resonance captures in multifrequency systems, one can also refer to Bakhtin (1986), Lochak and Meunier (1988), Dodson et al. (1989) and Neishtadt (1997, 1999).

4.2. Numerical observations of LCO triggering mechanism

In this section, we study the LCO triggering mechanism due to aeroelastic instability numerically, utilizing the complex-valued slow-flow equations (13) with the optimal initial conditions (see Section 3.2) by which reasonable validity of the approximation can be achieved.

First, we examine the dynamics of the system at subcritical reduced speeds. Fig. 16(a) depicts the heave and pitch responses at a subcritical reduced speed ($\Theta = 0.5$), normalized by their respective maximum amplitudes in order to compare their frequency contents. Apparent existence of 1:2 IR (i.e., $\omega_{\text{pitch}} \approx 2\omega_{\text{heave}}$) was mentioned in Section 3.1 from the wavelet transform analysis (Fig. 5). In addition, occurrence of 1:1 RCs was also suggested. One may observe the occurrence of these two resonance interactions from the plot of Fig. 16(a). Considering the dominant frequencies in each response up to $\tau \approx 100$, we approximately compute the frequency ratio of heave to pitch modes as one-to-two; for later times these two responses become one-to-one and out-of-phase as shown in the zoomed plot.

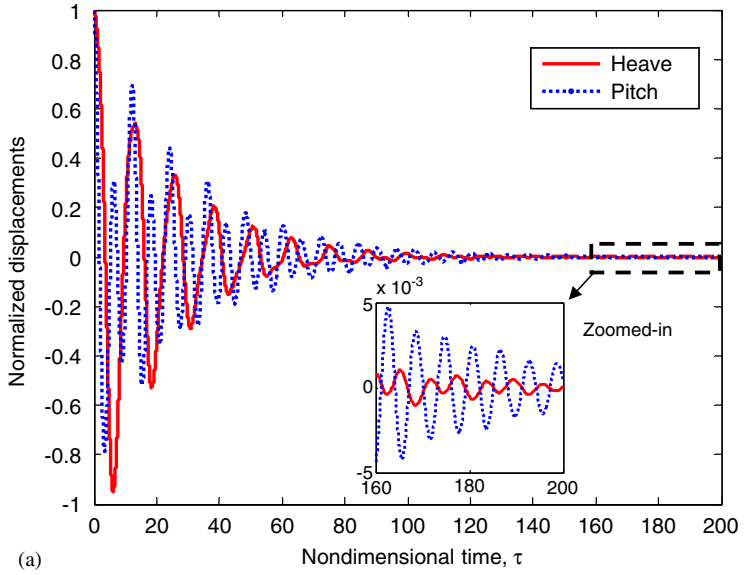

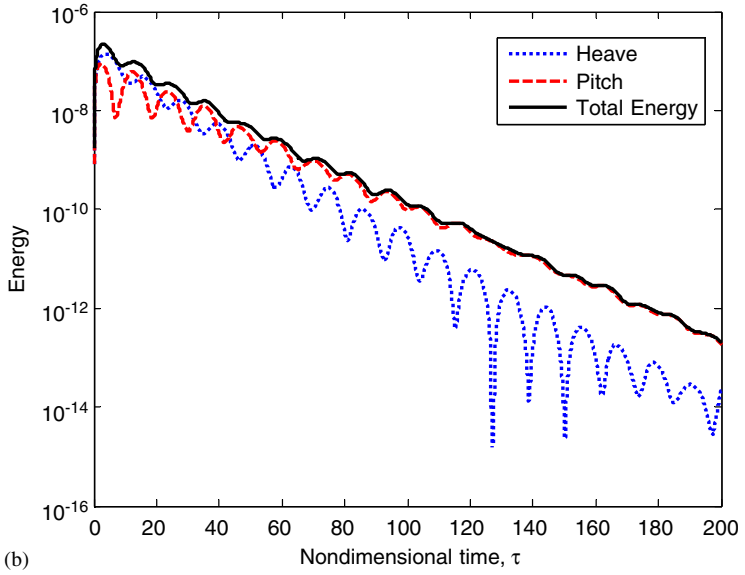

Fig. 16. Responses at subcritical speed ($\Theta = 0.5$). (a) Normalized heave and pitch responses, (b) energy variation with respect to time, (c) likewise phase differences in time, (d) likewise phase differences in phase plane, (e) phase interactions between different frequency components in time, (f) different phase interactions in phase plane, and (g) instantaneous frequencies; initial conditions are $(y(0), \alpha(0), y'(0), \alpha'(0)) = (10^{-3}, 10^{-3}, 0, 0)$.

The existence of 1:1 RCs can be verified by the phase analysis depicted in Fig. 16(c)–(f). We note that phase interactions with the HF component do not exist in essence and thus they are meaningless in the phase analysis at subcritical speeds (indeed, from Fig. 5 we deduced that there are no HF components in both responses). Note the wandering behavior of ϕ_{56} in Fig. 16(c), and the time-like behaviors of the phase interactions of MF components with HF components in Fig. 16(e) and (f). If we examine the phase interactions between the LF heave and LF pitch components, ϕ_{12}, and between the MF heave and MF pitch components, ϕ_{34}, we clearly establish their non-time-like behaviors in time domain (Fig. 16(c)), revealed in the form of spirals in the phase space (Fig. 16(d)); we conclude that these phase differences are not 'fast' angles so they may not be averaged out of the dynamics. On the contrary, their slow (non-time-like) temporal evolution indicates that the corresponding modes are involved in 1:1 resonance captures.

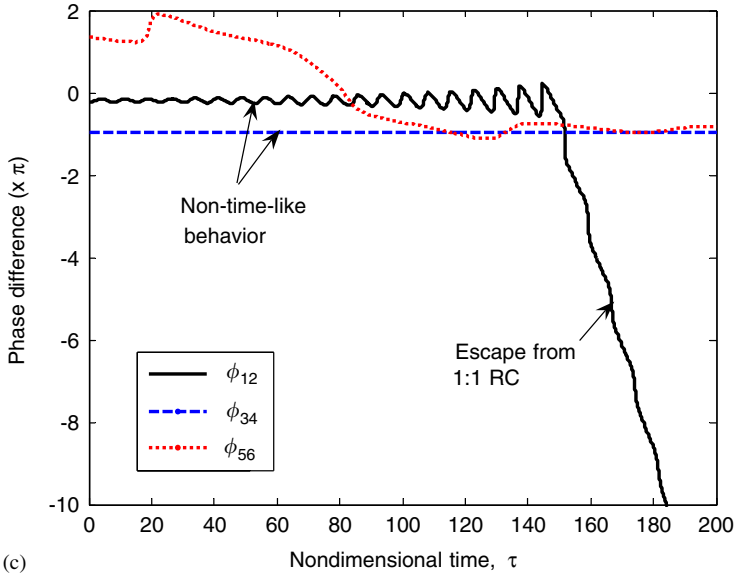

(c)

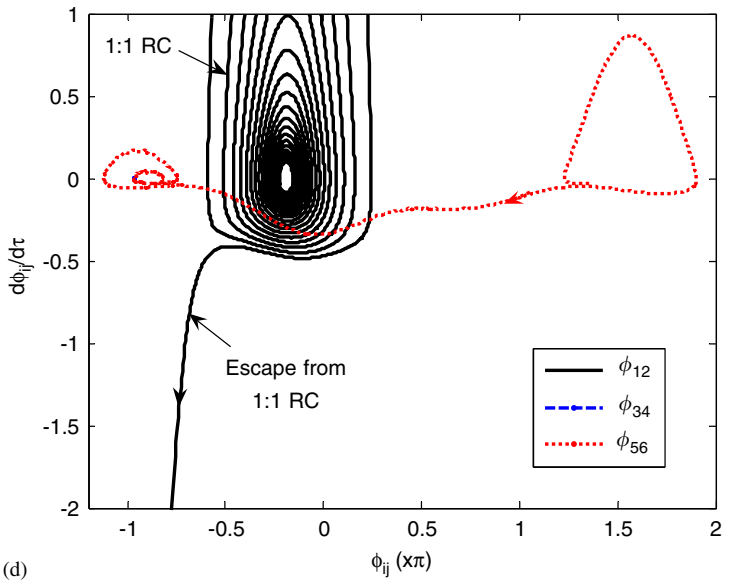

(d)

Fig. 16. (*Continued*)

By time-like phase variables we denote monotonically increasing or decreasing time responses so that those variables can be regarded as fast time variables by the relation $\vartheta \approx \omega t$ where ϑ is a phase variable, ω a frequency, and t the time variable (Sanders and Verhulst, 1985). Typically, such fast, time-like phase variables can be removed by applying averaging (see Section 4.3 regarding *partial averaging*). However, in the neighborhood of a resonance manifold, non-time-like behavior of the phase variables occurs, rendering them slow-varying and preventing their elimination from the equations of motion by direct averaging; in mathematical terms, the failure of the averaging theorem is due to the vanishing of a denominator in the averaged equations or, equivalently, due to the slow variation of the phase difference between the two harmonic components considered. Returning to the results of Fig. 16, the phase interaction between likewise MF components is slowly varying (as evidenced by its nearly straight line variation in Fig. 16(c)), while the corresponding phase difference between likewise LF components indicates escape from the 1:1 RC at $\tau \approx 150$.

The utilization of these phase interactions as evidence for IR or RCs is confirmed by the instantaneous frequencies of Fig. 16(g), computed by the following relations [see also the decomposition (9) with the complex variables (12) and the

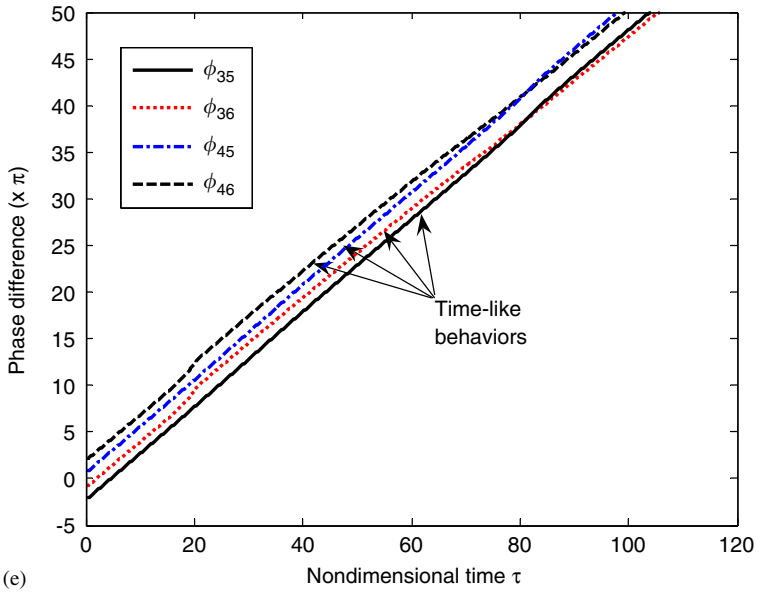

(e)

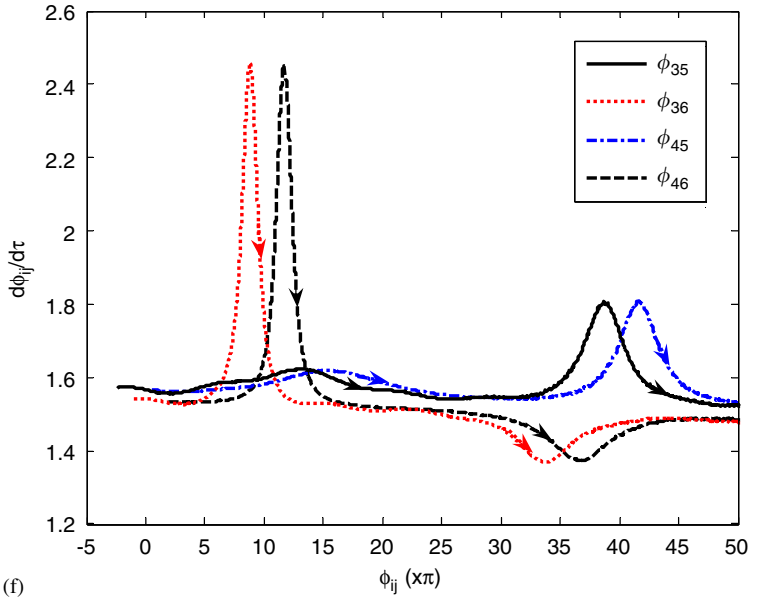

(f)

Fig. 16. (*Continued*)

polar coordinate transformations],

$$\omega_1^h(\tau) = \Omega + \beta_1'(\tau), \quad \omega_2^h(\tau) = 1 + \beta_3'(\tau), \quad \omega_3^h(\tau) = 3 + \beta_5'(\tau),$$
$$\omega_1^z(\tau) = \Omega + \beta_2'(\tau), \quad \omega_2^z(\tau) = 1 + \beta_4'(\tau), \quad \omega_3^z(\tau) = 3 + \beta_6'(\tau), \tag{26}$$

where $\beta_k = \tan^{-1}(\mathrm{Im}\,\varphi_k/\mathrm{Re}\,\varphi_k)$, $k = 1,\ldots,6$, and their derivatives regarded as slow frequency corrections to the fast dominant values (Zniber and Quinn, 2003).

For the 1:2 IR between heave and pitch modes, $\omega_2^z(\tau)$ is compared to $2\omega_1^h(\tau)$. Then, we check that the frequency relation, $\omega_2^z - 2\omega_1^h \approx 0$, persists in the entire time interval, which clearly implies the occurrence of 1:2 IR. We remark that this internal resonance is possible only because of our choice of a specific ratio between the natural frequencies, i.e., $\Omega = 0.5$. On the other hand, comparing $\omega_1^h(\tau)$ and $\omega_1^z(\tau)$, and $\omega_2^h(\tau)$ and $\omega_2^z(\tau)$, we clearly verify that 1:1 RCs and also

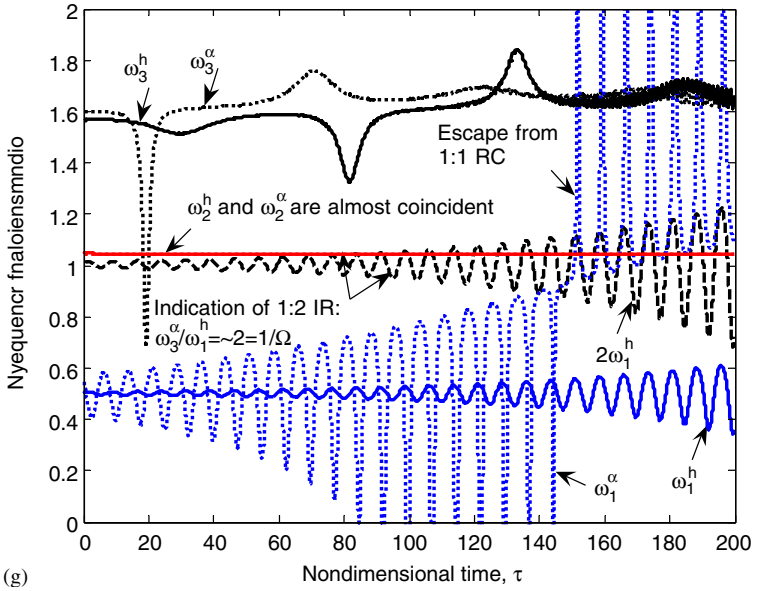

Fig. 16. (*Continued*)

escape from 1:1 RC in likewise LF components occur. Then, it is natural that we observe energy exchanges between heave and pitch modes such that the two modes are in an internal resonance with dissipation [see Fig. 16(b), (Greenlee and Snow, 1975)].

Now we explore the LCO triggering mechanism at supercritical flow speeds, using similar arguments. Basically, the triggering mechanism is composed of three main stages as discussed in wavelet transform analysis in Section 3.1. The classification is established by studying energy exchanges between heave and pitch modes (Fig. 17(b)), phase interactions between dominant frequency components (Fig. 17(c)–(f)), and the corresponding instantaneous frequencies (Fig. 17(g)). We refer to these three stages as Stages I, II, and III, with main corresponding features, one-to-one transient resonance captures (1:1 TRCs), escape from the 1:1 TRCs, and finally three-to-one permanent resonance captures (3:1 PRC), respectively. Each of these regimes for a specific supercritical reduced speed (i.e., $\Theta = 0.95$) is considered in detail below.

Stage I. Initial transients (up to $\tau \approx 20$) involves a 1:2 IR (Fig. 17(g)) which may initially cause strong energy exchanges between the heave and pitch modes (Fig. 17(b)). Then, these transients are driven quickly into 1:1 resonance capture regimes. Comparing the time responses (Fig. 17(a)), we find that they show in-phase, 1:1 resonance captures after the initial transients; and amplitudes of both modes (and thus the respective energies) are increasing. 1:1 RCs are much clearer in terms of instantaneous energy exchanges between modes (Fig. 17(b)); energies in both modes are raised until the energy of the heave mode reaches its maximum at the end of the Stage I.

In-phase 1:1 resonance capture has been reported as one of the fundamental mechanisms for *nonlinear energy pumping* (Kerschen et al., 2005), whereby, a major portion of the energy in a primary system is transferred irreversibly to an attached nonlinear subsystem, which is termed nonlinear energy sink (NES). In analogy, the pitch mode can be regarded as a primary system, and the heave mode as the NES where the energy is irreversibly transferred.

Our aeroelastic model possesses a positive damping component in the heave mode and negative damping in the pitch mode. Thus, unlike the usual nonlinear energy pumping phenomenon, energies in both modes increase during the 1:1 resonance captures. Besides, energy dissipation by the heave mode (as for the NES) plays no significant role in the competition between the two damping mechanisms. This also explains the viewpoint that *the initial excitation of the heave mode acts or triggers initiation and development of the pitch mode*. It is remarkable that the *nonlinear beating phenomenon*, which is caused by 1:2 IR (Nayfeh and Mook, 1979), was reported as the most efficient mechanism to transfer or initiate nonlinear energy pumping (Kerschen et al., 2005). That is why the short occurrence of 1:2 IR initially makes possible the maximum energy transfer. 1:1 RCs are verified by non-time-like behaviors of the phase differences between likewise frequency components (Fig. 17(c)), and spirals formed in the projection of the phase space (Fig. 17(d)).

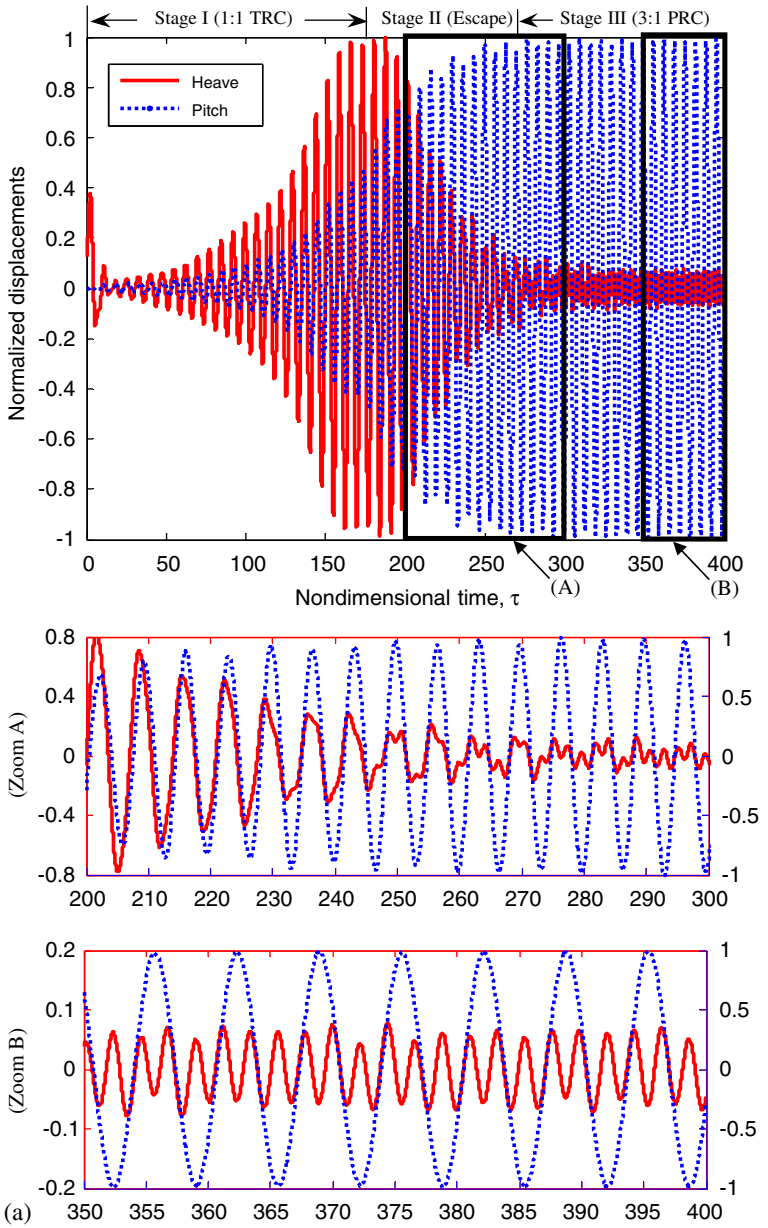

Fig. 17. Responses at supercritical speed ($\Theta = 0.95$). (a) Normalized heave and pitch responses, (b) energy variation with respect to time, (c) likewise phase differences in time, (d) likewise phase differences in phase plane, (e) phase interactions between different frequency components in time, (f) different phase interactions in phase plane, and (g) instantaneous frequencies; initial conditions are $(y(0), \alpha(0), y'(0), \alpha'(0)) = (10^{-3}, 10^{-3}, 0, 0)$.

In particular, the instantaneous frequencies shown in Fig. 17(g) indicate 1:1 RCs, since the frequencies of likewise frequency components lie, on average, very close to each other, following straight lines whereas in later times some of the components show *frequency shifting* (Zniber and Quinn, 2003) with increasing energy.

Stage II. Once the heave mode reaches its maximum, escape from 1:1 RCs occurs. Superimposed time responses show the transitions (Zoom A in Fig. 17(a)); the in-phase 1:1 RCs turn to 3:1 RCs at the end gradually as the heave and pitch amplitude decreases and increases, respectively. Thus the energy exchanges between the two modes (Fig. 17(b)) follows

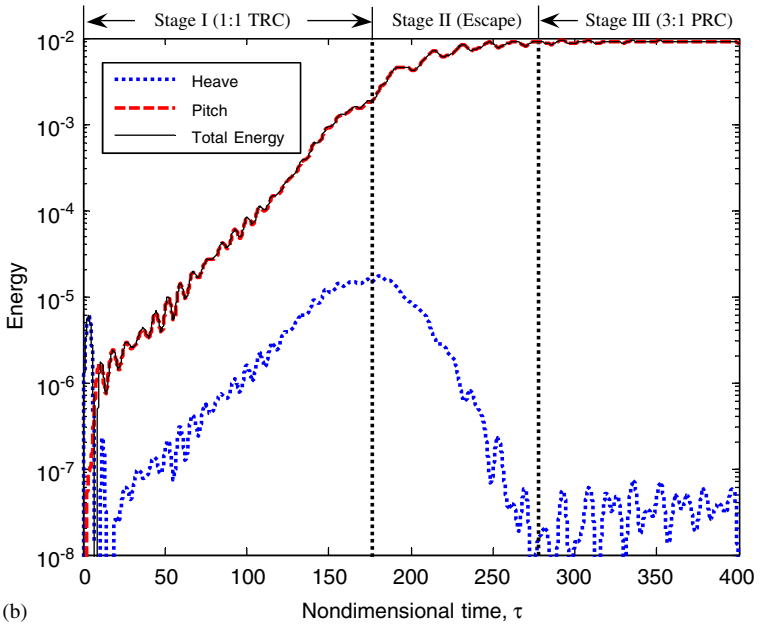

Fig. 17. (*Continued*)

the typical behavior of escape from in-phase 1:1 RC (Kerschen et al., 2005). Time-like behaviors of likewise phase differences (with ϕ_{56} the most prominent; Fig. 17(c)), and escaping from spirals in projected phase planes (Fig. 17(d)) confirm escape from 1:1 RCs. In the meanwhile, phase differences between MF heave and HF heave, and between MF pitch and HF heave show no more time-like behaviors, which is a precursor of 3:1 PRCs (Fig. 17(e)). Finally, this escape from 1:1 RCs is evident in terms of instantaneous frequencies (Fig. 17(g)).

Stage III. As a result of the escape at Stage II, the steady-state dynamics finally settles into 3:1 PRCs. Examining the zoomed-in plot of the responses (Fig. 17(a)), we can easily establish the frequency relation between the two modes as

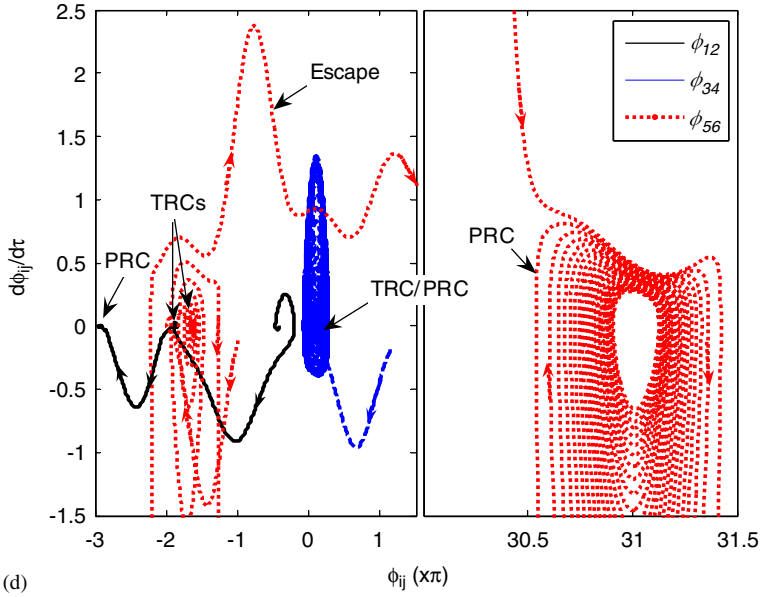

(d)

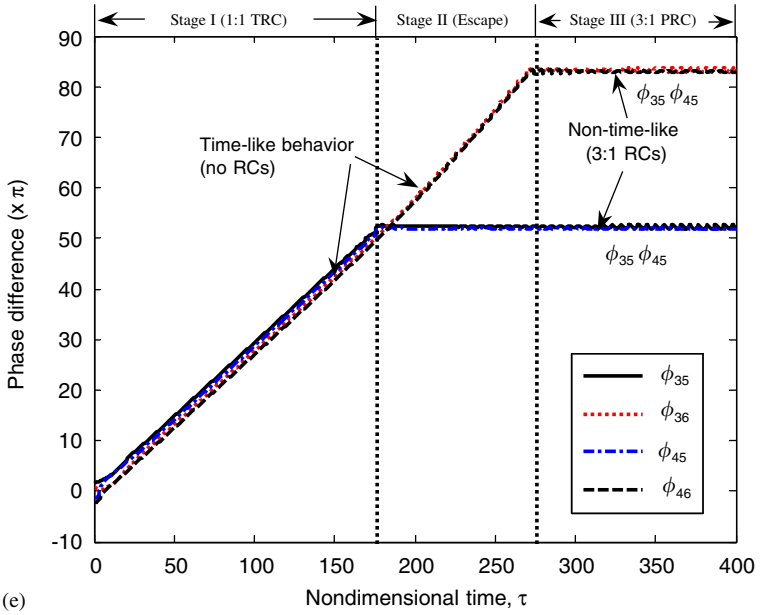

(e)

Fig. 17. (*Continued*)

nearly 3:1, and the occurrence of in-phase oscillations. The energy exchanges between heave and pitch modes become balanced, on average, and mostly imparted to the pitch mode (Fig. 17(b)). Resonance captures can be verified similarly as in Stages I and II, i.e., by means of non-time-like phase behaviors and spirals in the phase space, as well as in terms of instantaneous frequencies. In particular, comparing $3\omega_2^z(\tau)$ and $\omega_3^h(\tau)$ at this stage, we can find a good alignment between them on average; i.e., $3\omega_2^z - \omega_3^h \approx 0$ (Fig. 17(g)).

One thing to note is that the HF heave (or the steady-state resonance frequency component) undergoes upward frequency shift so that 3:1 PRC to MF pitch is made possible, as energy is continuously fed from the flow into the system. It is also remarkable that the likewise phase differences in Fig. 17(c) and (d) at this stage imply the existence of 1:1 RCs.

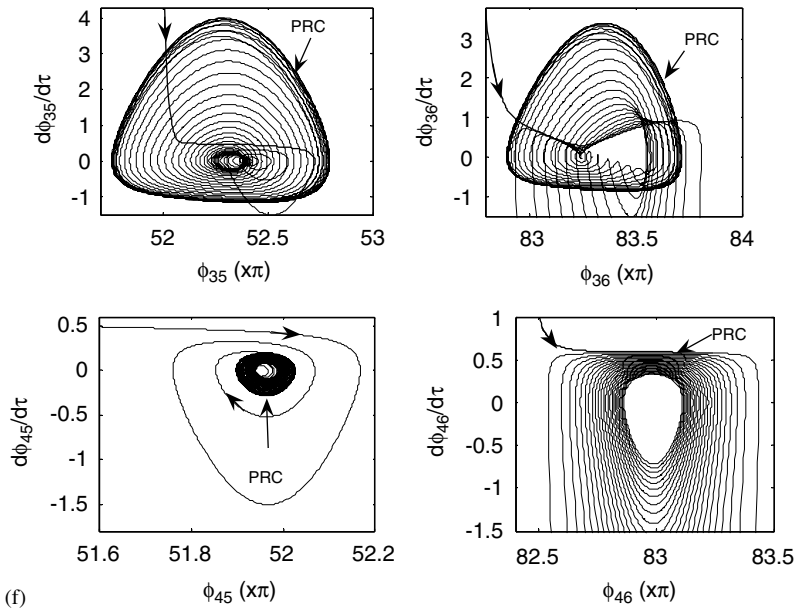

(f)

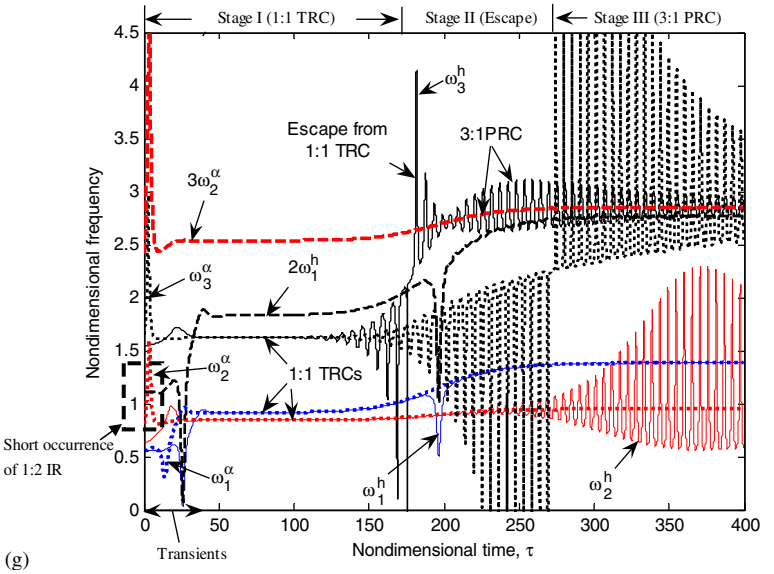

(g)

Fig. 17. (*Continued*)

4.3. *Analytical proof of LCO triggering mechanism*

In this section, we prove analytically the LCO triggering mechanism observed previously. Employing partial averaging which is a local analysis, we will perform averaging only for non-resonant (fast) phase angles that possess time-like behavior. In this way, we can remove the time-like phase variables, and achieve a *reduced-order model* (Zniber and Quinn, 2003).

We consider the analytical resonance captures in terms of numerical integration of the reduced-order model derived by the partial averaging at each stage of the analysis. Then, the order of approximation and its validity on the time scale can be verified when escape occurs. For the proof of PRC at Stage III, existence of steady-state equilibrium points of the reduced-order model will serve as a necessary (but not sufficient) condition for PRCs (Quinn, 1997a; Zniber and Quinn, 2003; Burns and Jones, 1993; Kath, 1983a, b).

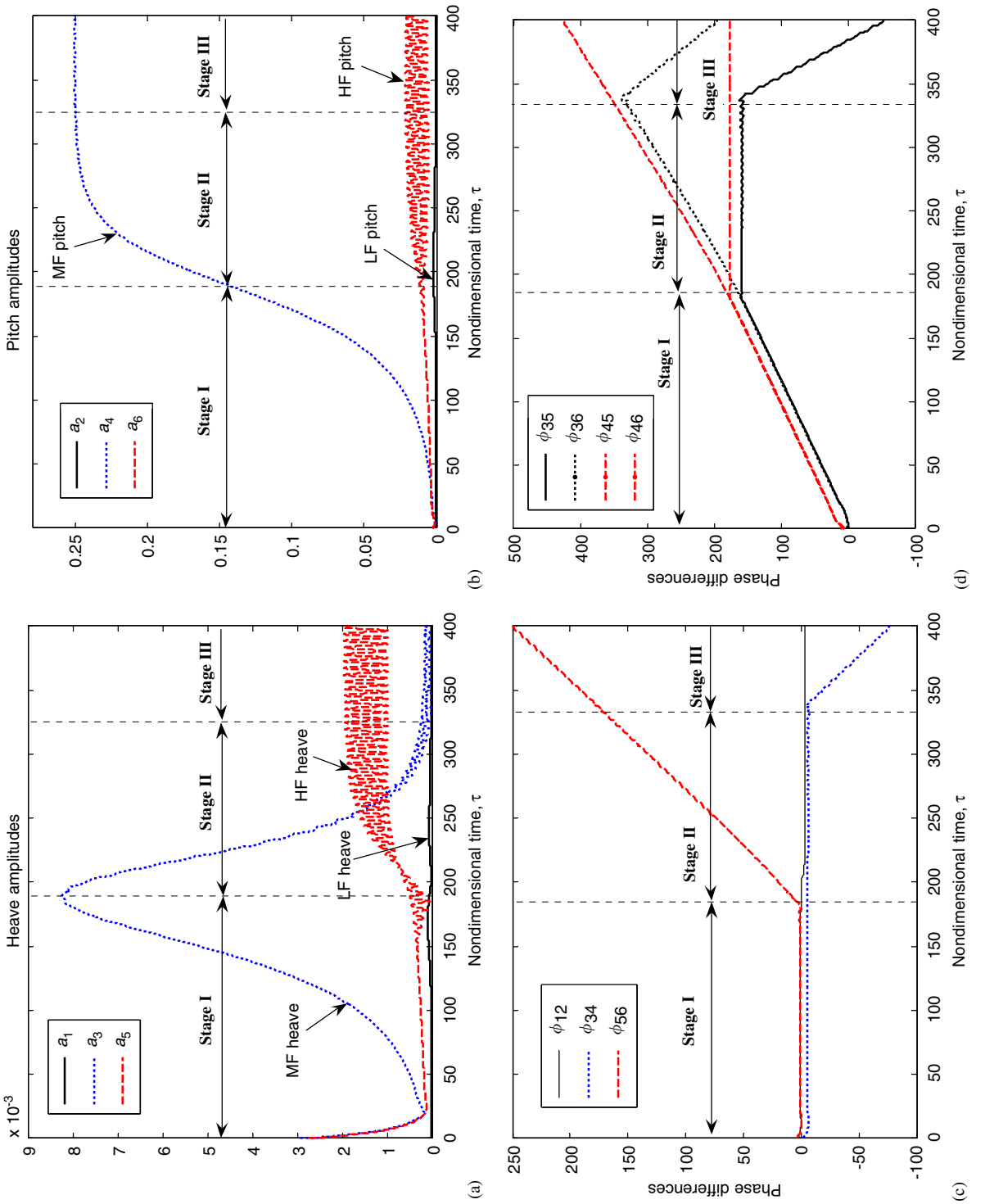

Fig. 18. Amplitude and phase responses computed from the averaged system (16) for a supercritical reduced velocity ($\Theta = 0.95$); initial conditions are $(y(0), \alpha(0), y'(0), \alpha'(0)) = (10^{-3}, 10^{-3}, 0, 0)$.

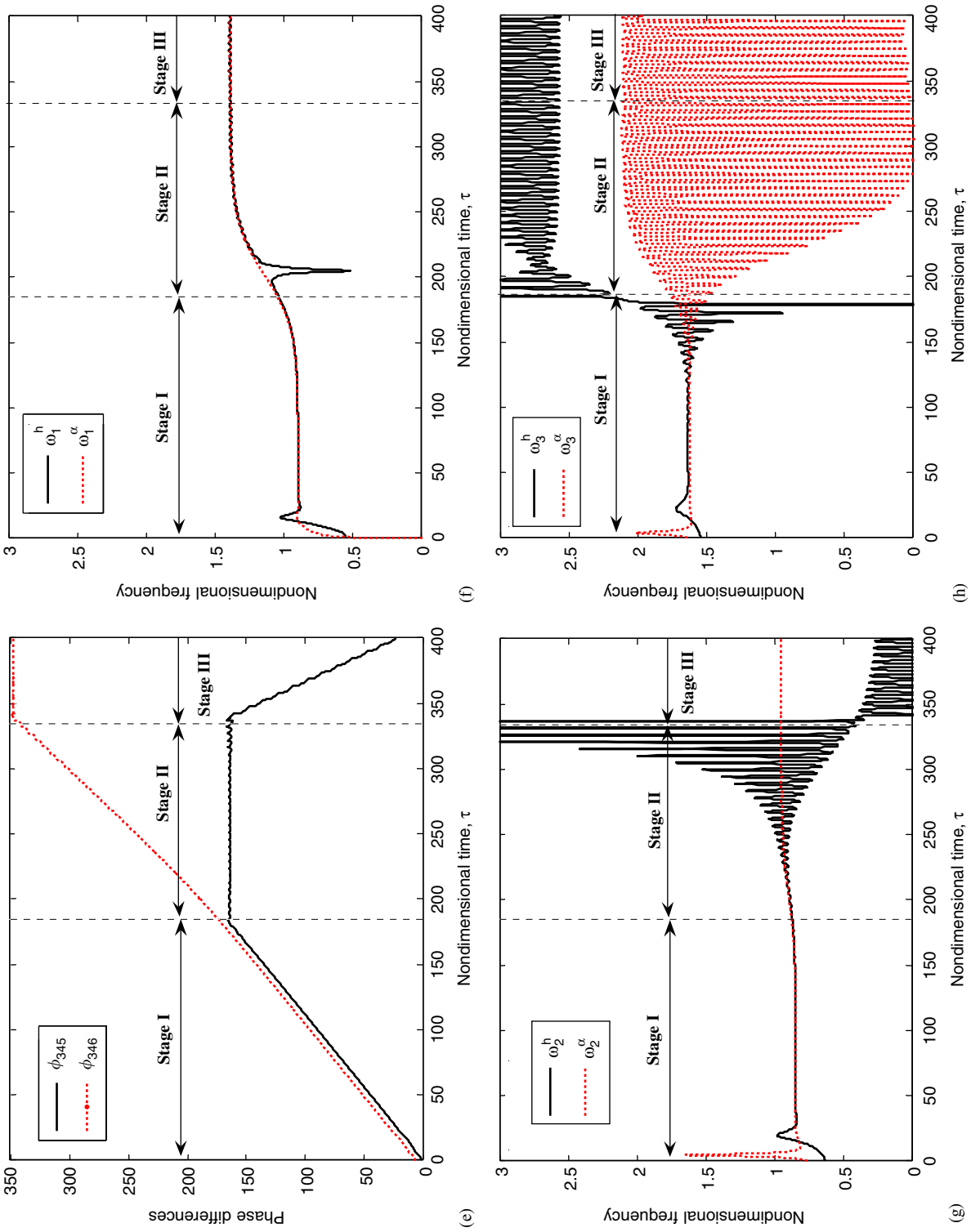

Fig. 18. (*Continued*)

Since the averaged system possesses sensitive dependence on initial conditions as explained in Section 3.3 due to the complexity of the phase space (see Figs. 12 and 13), optimal initial conditions for the slow-flow modulation equations in polar form (20) will be utilized. As a result, we may deduce different phase behaviors and different steady states (Fig. 18(c) and (d)) than those in Fig. 17 which were computed using the optimal initial conditions for the complex-valued modulation equations (13).

Figs. 18(a) and (b) show amplitude envelopes of heave and pitch components, respectively. We may expect that dominant contribution to the initial triggering of LCOs comes from MF heave so that it develops the likewise counterpart, MF pitch at Stage I. Then, from Stage II until the dynamics reaches its steady state, MF pitch together with MF heave act as the driving mechanism to further raise the amplitude of HF heave. This intuition is visualized in the phase responses.

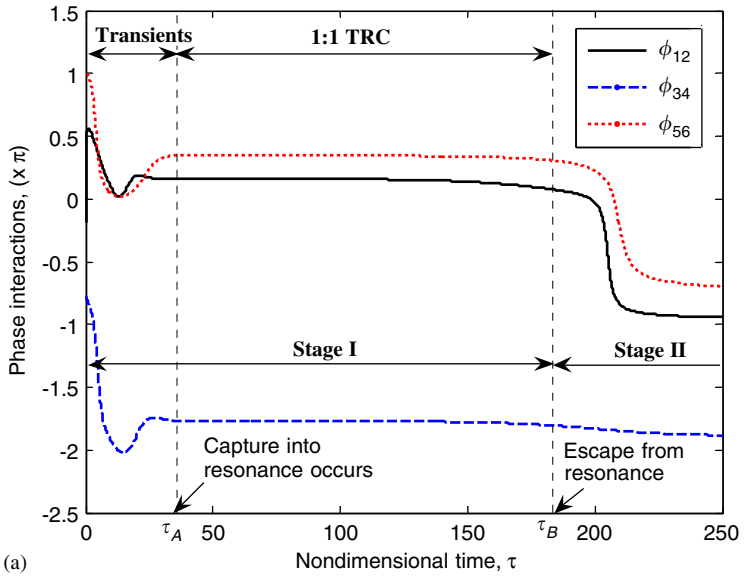

Fig. 19. Analytic resonance captures at Stage I ($\Theta = 0.95$): (a) phase interaction, (b) frequency shifting, (c) heave amplitude components, and (d) pitch amplitude components; initial conditions are $(y(0), \alpha(0), y'(0), \alpha'(0)) = (10^{-3}, 10^{-3}, 0, 0)$.

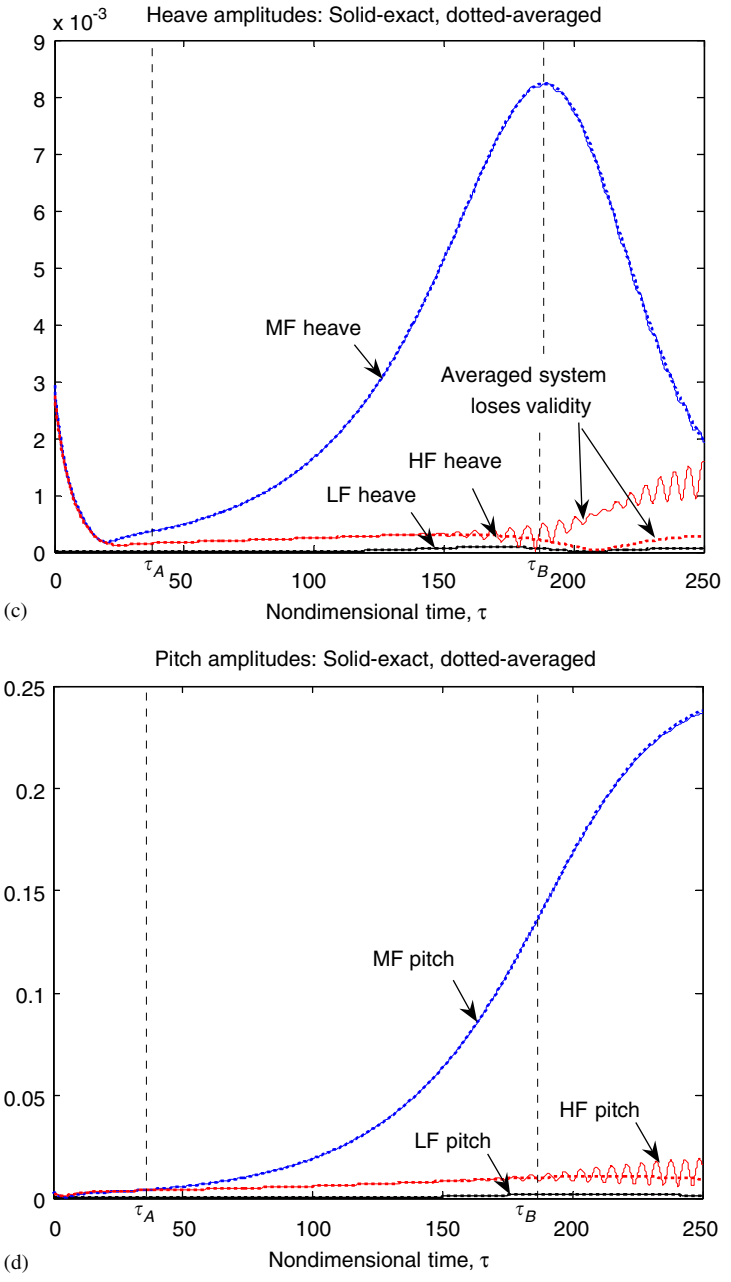

Fig. 19. (*Continued*)

The initial triggering is expressed by non-time-like behaviors of the likewise phase differences (and thus by 1:1 RCs) at Stage I (Fig. 18(c)). On the other hand, time-like responses in the other phase differences imply that no other effective triggering mechanisms exist. At Stage II, escape from likewise HF components occurs while the other likewise frequency components are still in 1:1 RCs. Non-time-like behaviors of the phase interactions between MF heave and HF heave (i.e., ϕ_{35}) and between MF pitch and HF heave (i.e., ϕ_{45}) support the previous argument. At steady state (i.e., Stage III), only phase differences between LF heave and LF pitch remain captured into 1:1 resonance while the other phase differences escape from 1:1 RCs. Indeed, only the phase interaction between MF pitch and HF heave keeps non-time-like behavior, which coincides with the numerical simulations (using the original dynamical system before averaging is applied).

In Fig. 18(f) and (h) the instantaneous frequency of each component is plotted by means of relations (26); however, this time the detuning frequency β'_k, $k = 1, \ldots, 6$ is directly computed from the slow-flow equations (20). Frequency locking between LF components persists almost during the entire time interval, and, in addition, the steady-state resonance frequencies show an upward frequency shift along with increasing energy input from the flow. Frequencies of MF components are kept in 1:1 RCs, on average, and become unlocked after Stage II, whereas those of HF components are unlocked just at the end of Stage I. In particular, the frequency shift in HF heave engages into another locking with three times of frequency of the MF pitch, as we already observed in the previous section.

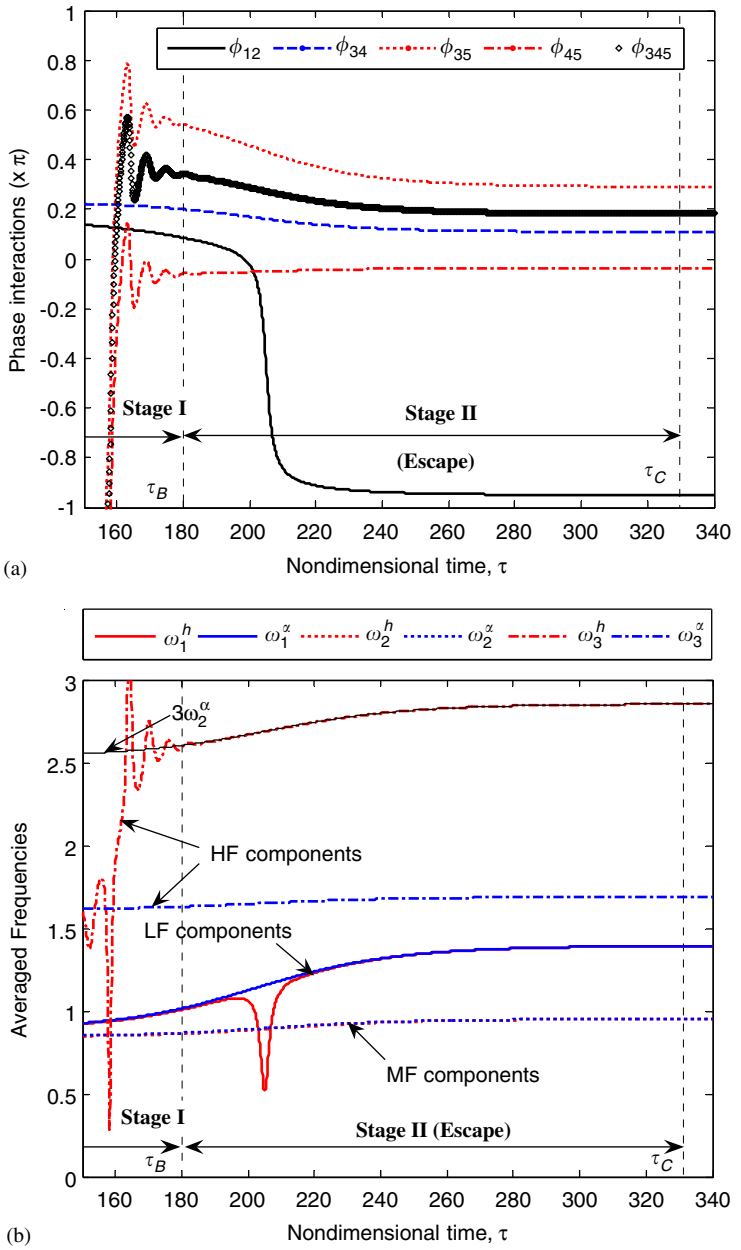

Fig. 20. Analytic resonance captures at Stage II ($\Theta = 0.95$): (a) phase interaction, (b) frequency shifting, (c) heave amplitude components, and (d) pitch amplitude components.

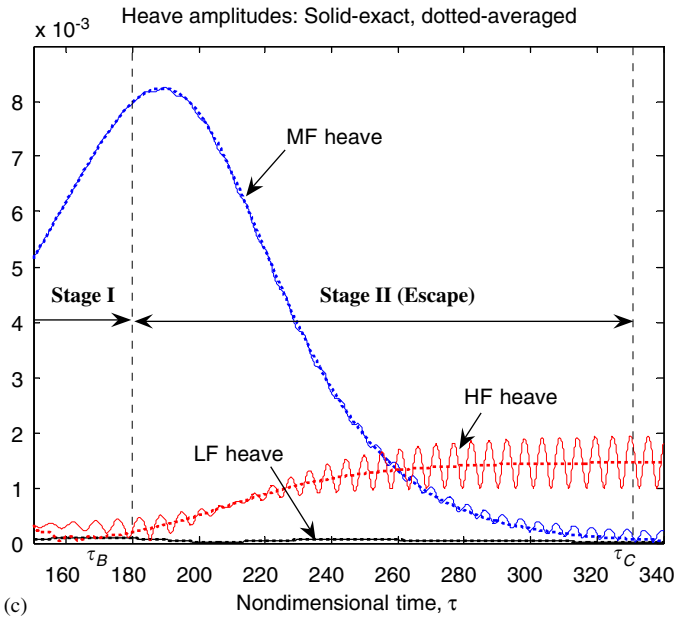

Fig. 20. (*Continued*)

Stage I. Performing partial averaging over all time-like phase variables except $\psi_I = (\phi_{12}, \phi_{34}, \phi_{56})$, we construct the reduced-order model for 1:1 TRCs of the form

$$a' = f_I(a; \psi_I), \quad \psi_I' = g_I(a; \psi_I), \tag{27}$$

where $a \in R^6$ and $\psi_I \in T^3 = S^1 \times S^1 \times S^1$. It will be sufficient to show numerically that there occurs an escape after some period of frequency locking. When solving the reduced-order model, we use the optimal initial conditions which are the same as those we used for the slow-flow equations (20). Then, we obtain the phase interactions depicted in Fig. 19(a) and (b) where τ_A and τ_B refer to the approximate time instants when the dynamics is captured into, and escape from RC. Hence, we definitely verify that there exist 1:1 TRCs at Stage I. When transition to escape occurs at τ_B,

the partially averaged system loses validity. This becomes clear when one compares the exact and averaged HF heave responses (Fig. 19(d)). The partially averaged system loses its validity when the escape occurs at τ_B. Frequency locking occurs only between likewise phase differences.

Stage II. We perform a similar analysis as for Stage I. In this case, we define the non-time-like variables as $\psi_{II} = (\phi_{12}, \phi_{34}, \phi_{35}, \phi_{45}, \phi_{345}) \in T^5$ and construct the reduced-order model in the form

$$a' = f_{II}(a; \psi_{II}), \quad \psi'_{II} = g_{II}(a; \psi_{II}). \tag{28}$$

We note that in this case there exist only three phases as independent variables. As for the initial conditions for (28), we pick the instant τ_B when the system enters Stage II, starting from the optimal initial conditions for (20). It is evident

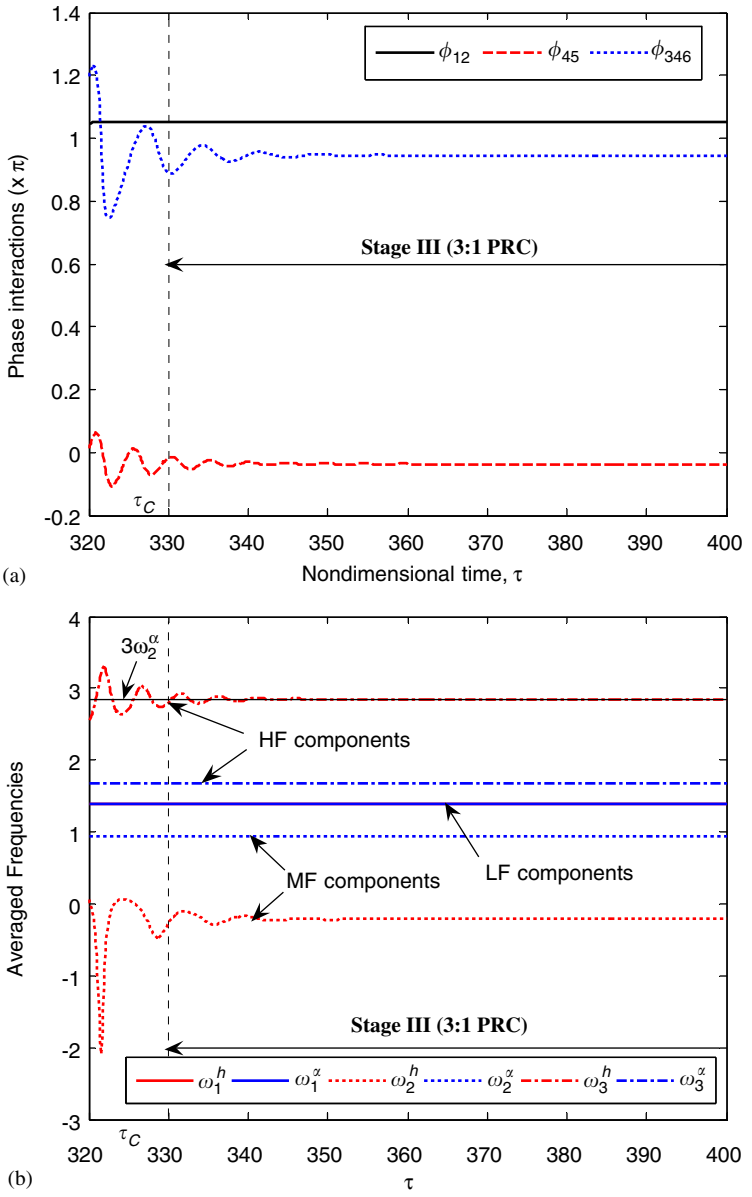

Fig. 21. Analytic resonance captures at Stage III ($\Theta = 0.95$): (a) phase interaction, (b) frequency shifting, (c) heave amplitude components, and (d) pitch amplitude components.

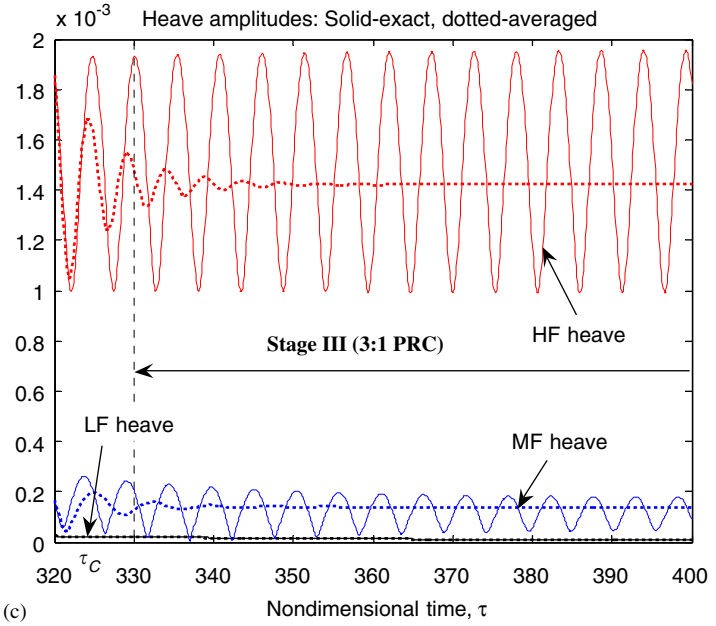

(c)

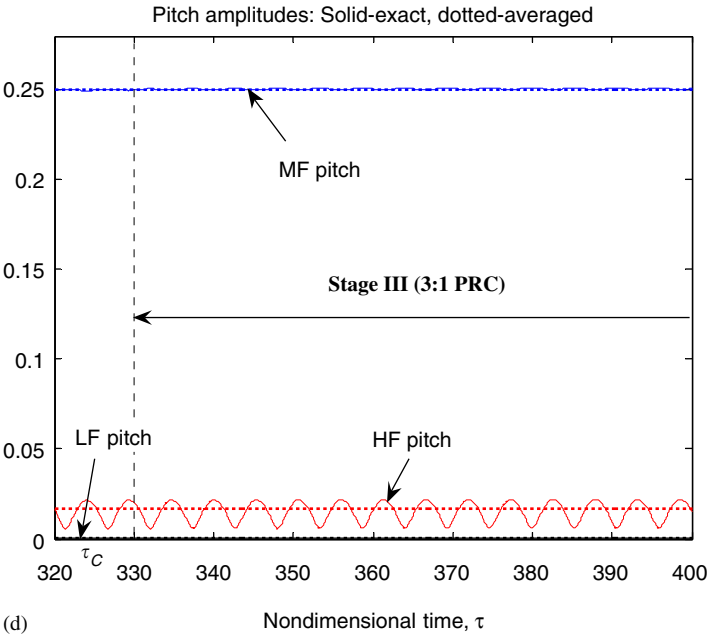

(d)

Fig. 21. (*Continued*)

(Fig. 20) that the dynamics is settling down into a steady-state motion at time instant τ_C. In particular, the (resonant) frequencies of the HF components shift upward to their original positions (i.e., ≈ 3) so that the system can attain 3:1 RCs. Note that the high-frequency modulations disappear through the partial averaging.

Stage III. We derive the reduced-order model with the non-time-like phase variables $\psi_{III} = (\phi_{12}, \phi_{45}, \phi_{346})$ such that

$$a' = f_{III}(a; \psi_{III}), \quad \psi'_{III} = g_{III}(a; \psi_{III}) \tag{29}$$

When solving the reduced-order model, we perform a similar analysis with Stage II, and then find that there exist equilibrium (or steady state) points as proof of PRCs. Recall that the time derivatives of the phase variables, β_k', $k = 1, \ldots, 6$, in (26) act as *detuning frequency* components. Therefore, instead of finding equilibrium conditions for detuning parameters as in Zniber and Quinn (2003), we focus on finding such conditions that $\beta_i' \approx \beta_{i+1}', i = 1, 3, 5$ for 1:1 resonance captures, and $3\beta_4' \approx \beta_5'$ for 3:1 resonance captures. In this way, we may define the interval where frequency locking occurs as evidence for resonance captures.

Fig. 21 finally shows the steady state (or PRC) in terms of the reduced-order model (29). Following Burns and Jones (1993) and Zniber and Quinn (2003), we may verify existence of PRCs by finding equilibria computed by the reduced-order model; that is, by examining the equilibria of pendulum-like equations obtained by partial averaging of the original equations in neighborhoods of resonance manifolds. It is still not so easy to manually compute the equilibria of the reduced model (29). Instead, we may verify their existence, for example, by examining Fig. 21(a)–(d), with convergence at steady state regarded as proof of existence of the corresponding equilibria. Besides, we already found some of these steady-state solutions by way of numerical continuation in Section 3.3. Thus, we may conclude that resonance captures are retained permanently, i.e., that PRCs exist.

5. Concluding remarks

We investigated the LCO triggering mechanisms in a two-dof wing model in subsonic flow by employing quasi-steady aerodynamics. Reviewing fundamental aspects of linear flutter theory, we established a slow-flow model based on multiphase averaging which exhibits good agreement with the original dynamics. Through the method of numerical continuation of equilibria, we analyzed the steady-state dynamics. The number of degenerate equilibria (i.e., not physically meaningful because they are valid only in lower-dimensional phase space) is suspected to exceed that of nondegenerate (but physically realizable) ones. Besides, the averaged system showed sensitive dependence on initial conditions due to the resulting complexity of the phase space. It is interesting to note that even at subcritical flow speeds 1:1 resonance captures occur and are responsible for strong energy exchanges between modes. We also found that the LCO triggering mechanism is composed of a series of one-to-one transient resonance capture, escape from capture, and then three-to-one permanent resonance capture. After exploring the triggering mechanism numerically at each stage, we proved our claims analytically by means of partial averaging.

Acknowledgments

This work was funded by AFOSR Contract FA9550-04-1-0073. GK would like to acknowledge grants from the Belgian National Fund for Scientific Research—FNRS, the Belgian Rotary District 1630, the Fulbright and Duesberg foundations which made his visit to NTUA and the University of Illinois possible.

Appendix A

A.1. Complex-valued modulation equations

$$\varphi_1' + \frac{1}{2}\left[\zeta_1 + \mathrm{j}\left(\Omega - \frac{k_{11}}{\Omega}\right)\right]\varphi_1 - \frac{\mathrm{j}k_{12}}{2\Omega}\varphi_2 - \frac{3\mathrm{j}}{8\Omega^3}(n_{11}\varphi_1|\varphi_1|^2 + n_{12}\varphi_2|\varphi_2|^2) - \frac{3\mathrm{j}}{4\Omega}(n_{11}\varphi_1|\varphi_3|^2 + n_{12}\varphi_2|\varphi_4|^2) - \frac{\mathrm{j}}{12\Omega}(n_{11}\varphi_1|\varphi_5|^2 + n_{12}\varphi_2|\varphi_6|^2) = 0, \tag{A.1}$$

$$\varphi_2' + \frac{1}{2}\left(\zeta_2 - \mathrm{j}\frac{k_{21}}{\Omega}\right)\varphi_1 + \frac{\mathrm{j}}{2}\left(\Omega - \frac{k_{22}}{\Omega}\right)\varphi_2 - \frac{3\mathrm{j}}{8\Omega^3}(n_{21}\varphi_1|\varphi_1|^2 + n_{22}\varphi_2|\varphi_2|^2) - \frac{3\mathrm{j}}{4\Omega}(n_{21}\varphi_1|\varphi_3|^2 + n_{22}\varphi_2|\varphi_4|^2) - \frac{\mathrm{j}}{12}(n_{21}\varphi_1|\varphi_5|^2 + n_{22}\varphi_2|\varphi_6|^2) = 0, \tag{A.2}$$

$$\varphi_3' + \frac{1}{2}[\zeta_1 + \mathrm{j}(1-k_{11})]\varphi_3 - \frac{\mathrm{j}k_{12}}{2}\varphi_4 - \frac{3\mathrm{j}}{4\Omega^2}(n_{11}\varphi_3|\varphi_1|^2 + n_{12}\varphi_4|\varphi_2|^2) - \frac{3\mathrm{j}}{8}(n_{11}\varphi_3|\varphi_3|^2 + n_{12}\varphi_4|\varphi_4|^2)$$
$$- \frac{\mathrm{j}}{12}(n_{11}\varphi_3|\varphi_5|^2 + n_{12}\varphi_4|\varphi_6|^2) + \frac{\mathrm{j}}{8}(n_{11}\varphi_3^{*2}\varphi_5 + n_{12}\varphi_4^{*2}\varphi_6) = 0, \tag{A.3}$$

$$\varphi_4' + \frac{1}{2}(\zeta_2 - \mathrm{j}k_{21})\varphi_3 + \frac{\mathrm{j}}{2}(1-k_{22})\varphi_4 - \frac{3\mathrm{j}}{4\Omega^2}(n_{21}\varphi_3|\varphi_1|^2 + n_{22}\varphi_4|\varphi_2|^2) - \frac{3\mathrm{j}}{8}(n_{21}\varphi_3|\varphi_3|^2 + n_{22}\varphi_4|\varphi_4|^2)$$
$$- \frac{\mathrm{j}}{12}(n_{21}\varphi_3|\varphi_5|^2 + n_{22}\varphi_4|\varphi_6|^2) + \frac{\mathrm{j}}{8}(n_{21}\varphi_3^{*2}\varphi_5 + n_{22}\varphi_4^{*2}\varphi_6) = 0, \tag{A.4}$$

$$\varphi_5' + \frac{1}{2}\left[\zeta_1 + \mathrm{j}\left(3 - \frac{k_{11}}{3}\right)\right]\varphi_5 - \frac{\mathrm{j}k_{12}}{6}\varphi_6 - \frac{\mathrm{j}}{4\Omega^2}(n_{11}\varphi_5|\varphi_1|^2 + n_{12}\varphi_6|\varphi_2|^2)$$
$$- \frac{\mathrm{j}}{4}(n_{11}\varphi_5|\varphi_3|^2 + n_{12}\varphi_6|\varphi_4|^2) - \frac{\mathrm{j}}{72}(n_{11}\varphi_5|\varphi_5|^2 + n_{12}\varphi_6|\varphi_6|^2) + \frac{\mathrm{j}}{8}(n_{11}\varphi_3^3 + n_{12}\varphi_4^3) = 0, \tag{A.5}$$

$$\varphi_6' + \frac{1}{2}\left(\zeta_2 - \mathrm{j}\frac{k_{21}}{3}\right)\varphi_5 + \frac{\mathrm{j}}{2}\left(3 - \frac{k_{22}}{3}\right)\varphi_6 - \frac{\mathrm{j}}{4\Omega^2}(n_{21}\varphi_5|\varphi_1|^2 + n_{22}\varphi_6|\varphi_2|^2) - \frac{\mathrm{j}}{4}(n_{21}\varphi_5|\varphi_3|^2 + n_{22}\varphi_6|\varphi_4|^2)$$
$$- \frac{\mathrm{j}}{72}(n_{21}\varphi_5|\varphi_5|^2 + n_{22}\varphi_6|\varphi_6|^2) + \frac{\mathrm{j}}{8}(n_{21}\varphi_3^3 + n_{22}\varphi_4^3) = 0. \tag{A.6}$$

A.2. Polar-form modulation equations

$$a_1' + \frac{\zeta_1}{2}a_1 - \frac{a_2}{2\Omega}\sin(\beta_1 - \beta_2)\left(k_{12} + \frac{3n_{12}}{4\Omega^2}a_2^2 + \frac{3n_{12}}{2}a_4^2 + \frac{n_{12}}{6}a_6^2\right) = 0, \tag{A.7}$$

$$a_2' + \frac{\zeta_2}{2}a_1\cos(\beta_1 - \beta_2) + \frac{a_1}{2\Omega}\sin(\beta_1 - \beta_2)\left(k_{21} + \frac{3n_{21}}{4\Omega^2}a_1^2 + \frac{3n_{21}}{2}a_3^2 + \frac{n_{21}}{6}a_5^2\right) = 0, \tag{A.8}$$

$$a_3' + \frac{\zeta_1}{2}a_3 - \frac{a_4}{2}\sin(\beta_3 - \beta_4)\left(k_{12} + \frac{3n_{12}}{2\Omega^2}a_2^2 + \frac{3n_{12}}{4}a_4^2 + \frac{n_{12}}{6}a_6^2\right) + \frac{n_{11}}{8}a_3^2a_5\sin(3\beta_3 - \beta_5)$$
$$+ \frac{n_{12}}{8}a_4^2a_6\sin(\beta_3 + 2\beta_4 - \beta_6) = 0, \tag{A.9}$$

$$a_4' + \frac{\zeta_2}{2}a_3\cos(\beta_3 - \beta_4) + \frac{a_3}{2}\sin(\beta_3 - \beta_4)\left(k_{21} + \frac{3n_{21}}{2\Omega^2}a_1^2 + \frac{3n_{21}}{4}a_3^2 + \frac{n_{21}}{6}a_5^2\right)$$
$$+ \frac{n_{22}}{8}a_4^2a_6\sin(3\beta_4 - \beta_6) + \frac{n_{21}}{8}a_3^2a_5\sin(2\beta_3 + \beta_4 - \beta_5) = 0, \tag{A.10}$$

$$a_5' + \frac{\zeta_1}{2}a_5 - \frac{a_6}{6}\sin(\beta_5 - \beta_6)\left(k_{12} + \frac{3n_{12}}{2\Omega^2}a_2^2 + \frac{3n_{12}}{2}a_4^2 + \frac{n_{12}}{12}a_6^2\right) - \frac{n_{11}}{8}a_3^3\sin(3\beta_3 - \beta_5)$$
$$- \frac{n_{12}}{8}a_4^3\sin(3\beta_4 - \beta_5) = 0, \tag{A.11}$$

$$a_6' + \frac{\zeta_2}{2}a_5\cos(\beta_5 - \beta_6) + \frac{a_5}{6}\sin(\beta_5 - \beta_6)\left(k_{21} + \frac{3n_{21}}{2\Omega^2}a_1^2 + \frac{3n_{21}}{2}a_3^2 + \frac{n_{21}}{12}a_5^2\right)$$
$$- \frac{n_{22}}{8}a_4^3\sin(3\beta_4 - \beta_6) - \frac{n_{21}}{8}a_3^3\sin(3\beta_3 - \beta_6) = 0, \tag{A.12}$$

$$a_1\beta_1' + \frac{a_1}{2\Omega}\left(\Omega^2 - k_{11} - \frac{3n_{11}}{4\Omega^2}a_1^2 - \frac{3n_{11}}{2}a_3^2 - \frac{n_{11}}{6}a_5^2\right)$$
$$- \frac{a_2}{2\Omega}\cos(\beta_1 - \beta_2)\left(k_{12} + \frac{3n_{12}}{4\Omega^2}a_2^2 + \frac{3n_{12}}{2}a_4^2 + \frac{n_{12}}{6}a_6^2\right) = 0, \tag{A.13}$$

$$a_2\beta_2' + \frac{a_2}{2\Omega}\left(\Omega^2 - k_{22} - \frac{3n_{22}}{4\Omega^2}a_2^2 - \frac{3n_{22}}{2}a_4^2 - \frac{n_{22}}{6}a_6^2\right) + \frac{\zeta_1}{2}a_1\,\sin(\beta_1-\beta_2) - \frac{a_1}{2\Omega}\cos(\beta_1-\beta_2)\left(k_{21} + \frac{3n_{21}}{4\Omega^2}a_1^2 + \frac{3n_{21}}{2}a_3^2 + \frac{n_{21}}{6}a_5^2\right) = 0, \tag{A.14}$$

$$a_3\beta_3' + \frac{a_3}{2}\left(1 - k_{11} - \frac{3n_{11}}{2\Omega^2}a_1^2 - \frac{3n_{11}}{4}a_3^2 - \frac{n_{11}}{6}a_5^2\right) - \frac{a_4}{2}\cos(\beta_3-\beta_4)\left(k_{12} + \frac{3n_{12}}{2\Omega^2}a_2^2 + \frac{3n_{12}}{4}a_4^2 + \frac{n_{12}}{6}a_6^2\right) + \frac{n_{11}}{8}a_3^2a_5\,\cos(3\beta_3-\beta_5) + \frac{n_{12}}{8}a_4^2a_6\,\cos(\beta_3+2\beta_4-\beta_6) = 0, \tag{A.15}$$

$$a_4\beta_4' + \frac{a_4}{2}\left(1 - k_{22} - \frac{3n_{22}}{2\Omega^2}a_2^2 - \frac{3n_{22}}{4}a_4^2 - \frac{n_{22}}{6}a_6^2\right) + \frac{\zeta_2}{2}a_3\,\sin(\beta_3-\beta_4) - \frac{a_3}{2}\cos(\beta_3-\beta_4)\left(k_{21} + \frac{3n_{21}}{2\Omega^2}a_1^2 + \frac{3n_{21}}{4}a_3^2 + \frac{n_{21}}{6}a_5^2\right) + \frac{n_{22}}{8}a_4^2a_6\,\cos(3\beta_4-\beta_6) + \frac{n_{21}}{8}a_3^2a_5\,\cos(2\beta_3+\beta_4-\beta_5) = 0, \tag{A.16}$$

$$a_5\beta_5' + \frac{a_5}{6}\left(9 - k_{11} - \frac{3n_{11}}{2\Omega^2}a_1^2 - \frac{3n_{11}}{2}a_3^2 - \frac{n_{11}}{12}a_5^2\right) - \frac{a_6}{6}\cos(\beta_5-\beta_6)\left(k_{12} + \frac{3n_{12}}{2\Omega^2}a_2^2 + \frac{3n_{12}}{2}a_4^2 + \frac{n_{12}}{12}a_6^2\right) + \frac{n_{11}}{8}a_3^3\,\cos(3\beta_3-\beta_5) + \frac{n_{12}}{8}a_4^3\,\cos(3\beta_4-\beta_5) = 0, \tag{A.17}$$

$$a_6\beta_6' + \frac{a_6}{6}\left(9 - k_{22} - \frac{3n_{22}}{2\Omega^2}a_2^2 - \frac{3n_{22}}{2}a_4^2 - \frac{n_{22}}{12}a_6^2\right) + \frac{\zeta_2}{2}a_5\,\sin(\beta_5-\beta_6) - \frac{a_5}{6}\cos(\beta_5-\beta_6)\left(k_{21} + \frac{3n_{21}}{2\Omega^2}a_1^2 + \frac{3n_{21}}{2}a_3^2 + \frac{n_{21}}{12}a_5^2\right) + \frac{n_{22}}{8}a_4^3\,\cos(3\beta_4-\beta_6) + \frac{n_{21}}{8}a_3^3\,\cos(3\beta_3-\beta_6) = 0. \tag{A.18}$$

References

Arnold, V.I., 1988. Dynamical Systems III (Encyclopedia of Mathematical Sciences). Springer, Berlin.

Bakhtin, V.I., 1986. Averaging in multifrequency systems. Functional Analysis and its Applications 20, 83–88 (English translation from Funkts. Anal. Prilozh. 20, 1–7, in Russian).

Belokonov, V., Zabolotnov, M., 2002. Estimation of the probability of capture into a resonance mode of motion for a spacecraft during its descent in the atmosphere. Cosmic Research 40, 467–478 (Translated from Kosmicheskie Issledovaniya 40, 503–514, 2002).

Blevins, R., 1990. Flow-Induced Vibration. Van Nostrand Reinhold, New York.

Bosley, D., Kevorkian, J., 1992. Adiabatic invariance and transient resonance in very slowly varying oscillatory Hamiltonian systems. SIAM Journal of Applied Mathematics 52, 494–527.

Bunton, R., Denegri Jr., C., 2000. Limit cycle oscillation characteristics of fighter aircraft. Journal of Aircraft, Engineering Note 37, 916–918.

Burns, T., Jones, C., 1993. A mechanism for capture into resonance. Physica D 69, 85–106.

Cattarius, J., 1999. Numerical wing/store interaction analysis of a parametric F16 wing. Ph.D. Thesis, Virginia Polytechnic Institute and State University.

Coller, B.D., Chamara, P.A., 2004. Structural non-linearities and the nature of the classic flutter instability. Journal of Sound and Vibration 277, 711–739.

Denegri Jr., C., 2000. Limit cycle oscillation flight test results of a fighter with external stores. Journal of Aircraft 37, 761–769.

Dhooge, A., Govaerts, W., Kuznetsov, Y.A., 2003. MATCONT: a Matlab package for numerical bifurcation analysis of ODEs. ACM Transactions on Mathematical Software 29, 141–164.

Dodson, M.M., Rynne, B.P., Vickers, J.A.G., 1989. Averaging in multifrequency systems. Nonlinearity 2, 137–148.

Dowell, E.H., Crawley, E.E., Curtiss Jr., H.C., Peters, D.A., Scanlan, R.H., Sisto, F., 1995. A Modern Course in Aeroelasticity. Kluwer Academic Publishers, Dordrecht.

Fung, Y., 1955. An Introduction to the Theory of Aeroelasticity. Wiley, New York.

Gilliatt, H., Strganac, T., Kurdila, A., 2003. An investigation of internal resonance in aeroelastic systems. Nonlinear Dynamics 31, 1–22.

Greenlee, W., Snow, R., 1975. Two-timing on the half line for damped oscillation equations. Journal of Mathematical Analysis and Applications 51, 394–428.

Guckenheimer, J., Holmes, P., 1983. Nonlinear Oscillations, Dynamical Systems, and Bifurcations of Vector Fields. Springer, New York.

Itin, A., Neishtadt, A., Vasiliev, A., 2000. Captures into resonance and scattering on resonance in dynamics of a charged relativistic particle in magnetic field and electrostatic wave. Physica D 141, 281–296.

Kath, W., 1983a. Necessary conditions for sustained reentry roll resonance. SIAM Journal of Applied Mathematics 43, 314–324.

Kath, W., 1983b. Conditions for sustained resonance II. SIAM Journal of Applied Mathematics 43, 579–583.

Keener, J., 1977. On the validity of the two-timing method for large times. SIAM Journal of Mathematical Analysis 8, 1067–1091.

Keener, J., 2000. Principles of Applied Mathematics: Transformation and Approximation. Westview Press, Boulder, CO.

Kerschen, G., Lee, Y.S., Vakakis, A.F., McFarland, D.M., Bergman, L.A., 2005. Irreversible passive energy transfer in coupled oscillators with essential nonlinearity. SIAM Journal of Applied Mathematics, in print.

Koon, W., Lo, M., Marsden, J., Ross, S., 2001. Resonance and capture of Jupiter comets. Celestial Mechanics and Dynamical Astronomy 81, 27–38.

Kubíček, M., 1976. Dependence of solution of nonlinear systems on a parameter. ACM Transactions on Mathematical Software 2, 98–107.

Lee, B.H.K., Desrochers, J., 1987. Flutter analysis of a two-dimensional airfoil containing structural nonlinearities. National Aeronautical Establishment, Aeronautical Report LR-618, National Research Council (Canada), No. 27833, Ottawa, ON, Canada.

Lee, B.H.K., LeBlanc, P., 1986. Flutter analysis of a two-dimensional airfoil with cubic nonlinear restoring force. National Aeronautical Establishment, Aeronautical Note 36, National Research Council (Canada) No. 25438, Ottawa, ON, Canada.

Lee, Y.S., Kerschen, G., Vakakis, A.F., Panagopoulos, P., Bergman, L.A., McFarland, D.M., 2005. Complicated dynamics of a linear oscillator with a light, essentially nonlinear attachment. Physica D 204, 41–69.

Lind, R., Snyder, K., Brenner, M., 2001. Wavelet analysis to characterise non-linearities and predict limit cycles of an aeroelastic system. Mechanical Systems and Signal Processing 15, 337–356.

Liu, L., Dowell, E., 2004. The secondary bifurcation of an aeroelastic airfoil motion: effect of high harmonics. Nonlinear Dynamics 37, 31–49.

Lochak, P., Meunier, C., 1988. Multiphase Averaging for Classical Systems: with Applications to Adiabatic Theorems. Springer, New York.

Manevitch, L., 2001. The description of localized normal modes in a chain of nonlinear coupled oscillators using complex variables. Nonlinear Dynamics 25, 95–109.

Nayfeh, A.H., Mook, D.T., 1979. Nonlinear Oscillations. Wiley, New York.

Neishtadt, A., 1975. Passage through a separatrix in a resonance problem with a slowly varying parameter. Journal of Applied Mathematics and Mechanics, PMM 39, 621–632.

Neishtadt, A., 1997. Scattering by resonances. Celestial Mechanics and Dynamical Astronomy 65, 1–20.

Neishtadt, A., 1999. On adiabatic invariance in two-frequency systems. In: Hamiltonian Systems with Three or More Degrees of Freedom, NATO ASI Series C 533. Kluwer Academic Publishers, Dordrecht, pp. 193–212.

O'Neil, T., Strganac, T., 1998. Aeroelastic response of a rigid wing supported by nonlinear springs. Journal of Aircraft 35, 616–622.

Quinn, D., 1997a. Resonance capture in a three degree-of-freedom mechanical system. Nonlinear Dynamics 14, 309–333.

Quinn, D., 1997b. Transition to escape in a system of coupled oscillators. International Journal of Non-Linear Mechanics 32, 1193–1206.

Sanders, J., Verhulst, F., 1985. Averaging Methods in Nonlinear Dynamical Systems. Springer, Berlin.

Sheta, E., Harrand, V., Thompson, D., Strganac, T., 2002. Computational and experimental investigation of limit cycle oscillations of nonlinear aeroelastic systems. Journal of Aircraft 39, 133–141.

Singh, S., Brenner, M., 2003. Limit cycle oscillation and orbital stability in aeroelastic systems with torsional nonlinearity. Nonlinear Dynamics 31, 435–450.

Vakakis, A.F., Gendelman, O., 2001. Energy pumping in nonlinear mechanical oscillators. Part II: Resonance capture. Journal of Applied Mechanics 68, 42–48.

Vakakis, A.F., Manevitch, L.I., Gendelman, O., Bergman, L.A., 2003. Dynamics of linear discrete systems connected to local essentially nonlinear attachment. Journal of Sound and Vibration 264, 559–577.

Zniber, A., Quinn, D., 2003. Frequency shifting in nonlinear resonant systems with damping. In: Proceedings of ASME 2003 Design Engineering Technical Conferences and Computers and Information in Engineering Conference, Chicago, IL, USA, DETC2003 / VIB-48444.